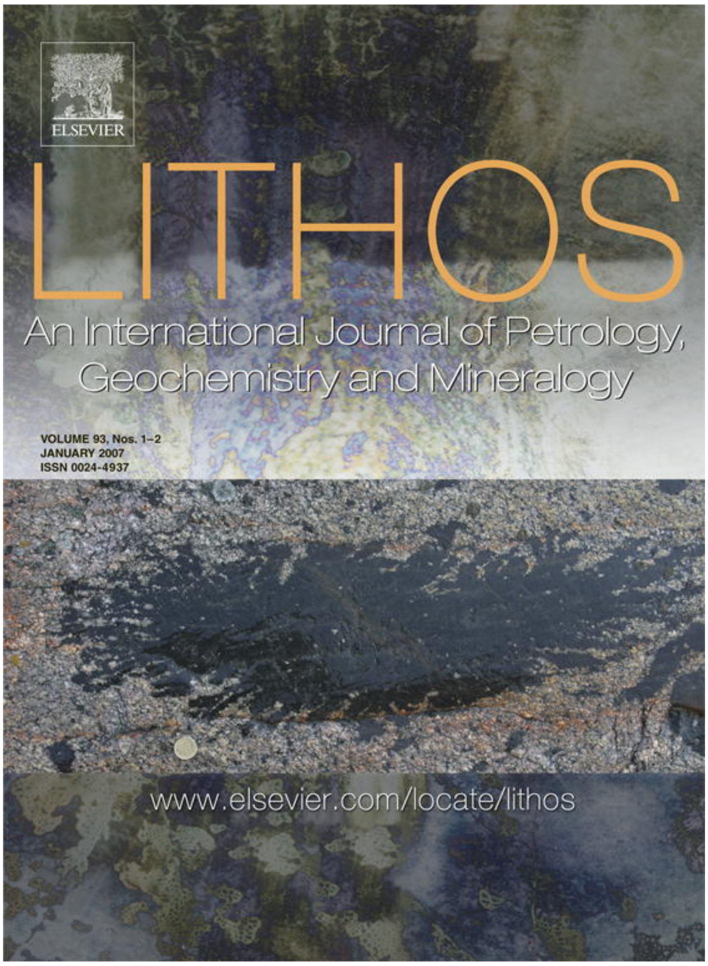
ELSEVIER
LITHOS
An International Journal of Petrology, Geochemistry and Mineralogy
VOLUME 93, Nos. 1–2
JANUARY 2007
ISSN 0024-4937
www.elsevier.com/locate/lithos

Available online at www.sciencedirect.com
ScienceDirect
Lithos 93 (2007) 17–38
LITHOS
www.elsevier.com/locate/lithos

Petrogenesis of the Puerto Edén Igneous and Metamorphic Complex, Magallanes, Chile: Late Jurassic syn-deformational anatexis of metapelites and granitoid magma genesis

M. Calderón [a,*], F. Hervé [a], H.-J. Massonne [b], C.G. Tassinari [c], R.J. Pankhurst [d], E. Godoy [e], T. Theye [b]

[a] Departamento de Geología, Universidad de Chile, Casilla 13518, Correo 21, Santiago, Chile
[b] Institut für Mineralogie und Kristallchemie, Universität Stuttgart, Azenbergstrasse 18, D-70174 Stuttgart, Germany
[c] Centro de Pesquisas Geocronológicas, Universidade de São Paulo, Rua do Lago 562, Cidade Universitaria, São Paulo, Brazil
[d] Visiting Research Associate, British Geological Survey, Keyworth, Nottingham NG12 5GG, UK
[e] Servicio Nacional de Geología y Minería, Avda. Santa María 0104, Santiago, Chile

Received 29 May 2005; accepted 22 March 2006
Available online 16 June 2006

Abstract

A suite of schists, gneisses, migmatites, and biotite granitoids from the Puerto Edén Igneous and Metamorphic Complex (PEIMC) and biotite–hornblende granitoids of the South Patagonian batholith (southern Chile) has been studied. For that purpose, the chemistry of minerals and the bulk rock composition of major and trace elements including Rb–Sr and Sm–Nd isotopes were determined. Mineralogical observations and geothermobarometric calculations indicate high-temperature and low-pressure conditions (ca. 600–700 °C and 3 to 4.5 kbar) for an event of metamorphism and partial melting of metapelites in Late Jurassic times (previously determined by SHRIMP U–Pb zircon ages). Structures in schists, gneisses, migmatites and mylonites indicate non-coaxial deformation flow during and after peak metamorphic and anatectic conditions. Andalusite schists and sillimanite gneisses yield initial $^{87}Sr/^{86}Sr$ ratios of up to 0.7134 and εNd_{150} values as low as − 7.6. Contemporaneous biotite granitoids and a coarse-grained orthogneiss have initial $^{87}Sr/^{86}Sr$ ratios between 0.7073 and 0.7089, and εNd_{150} values in the range − 7.6 to − 4.4. This indicates that metamorphic rocks do not represent the natural isotopic variation in the migmatite source. Thus, a heterogeneous source with a least radiogenic component was involved in the production of the biotite granitoids. The PEIMC is considered as a segment of an evolving kilometre-sized and deep crustal shear zone in which partial melts were generated and segregated into a large reservoir of magmas forming composite plutons in Late Jurassic times. A biotite–hornblende granodiorite and a muscovite–garnet leucogranite show initial $^{87}Sr/^{86}Sr$ ratios of 0.7048 and 0.7061, and εNd_{100} values of − 2.6 and − 1.8, respectively, and are thus probably related to Early Cretaceous magmas not involved in the anatexis of the metasedimentary rocks.

Keywords: Metapelites; Migmatites; Sr–Nd isotopes; Late Jurassic; Gondwana

1. Introduction

The formation of anatectic migmatites with pelitic or psammopelitic protoliths involves mainly muscovite and/

* Corresponding author. Tel.: +56 2 6784114.
E-mail address: caldera@esfera.cl (M. Calderón).

0024-4937/$ - see front matter © 2006 Published by Elsevier B.V.
doi:10.1016/j.lithos.2006.03.044

or biotite dehydration-melting reactions, with or without fluid influx, and partial melt back-reactions (e.g. Spear et al., 1999; Kriegsman, 2001; Milord et al., 2001; Otamendi and Patiño Douce, 2001). If deformation and melting are coeval, melts could move through the rocks by cyclic inflation and collapse of conduits, caused by build-up of melt pressure and periodic draining of the source (e.g. Brown and Solar, 1998; Weinberg, 1999). Melt segregation from the site of partial melting is followed either by in situ crystallisation, or by the later crystal fractionation and mobilisation of chanellised liquids with more evolved compositions (Milord et al., 2001). The study of these and corresponding processes is of special interest because of their inferred role as a link between high-grade metamorphism and the generation of larger-scale granitic bodies (e.g. Brown and D'Lemos, 1991; Solar and Brown, 2001).

Migmatites typically consist of lighter, intermediate and darker parts, usually named leucosome, mesosome and melanosome, which can be related to metamorphic and magmatic processes. The leucosome is considered to be the crystallisation product of an in situ felsic melt modified by cumulate products of partial crystallisation

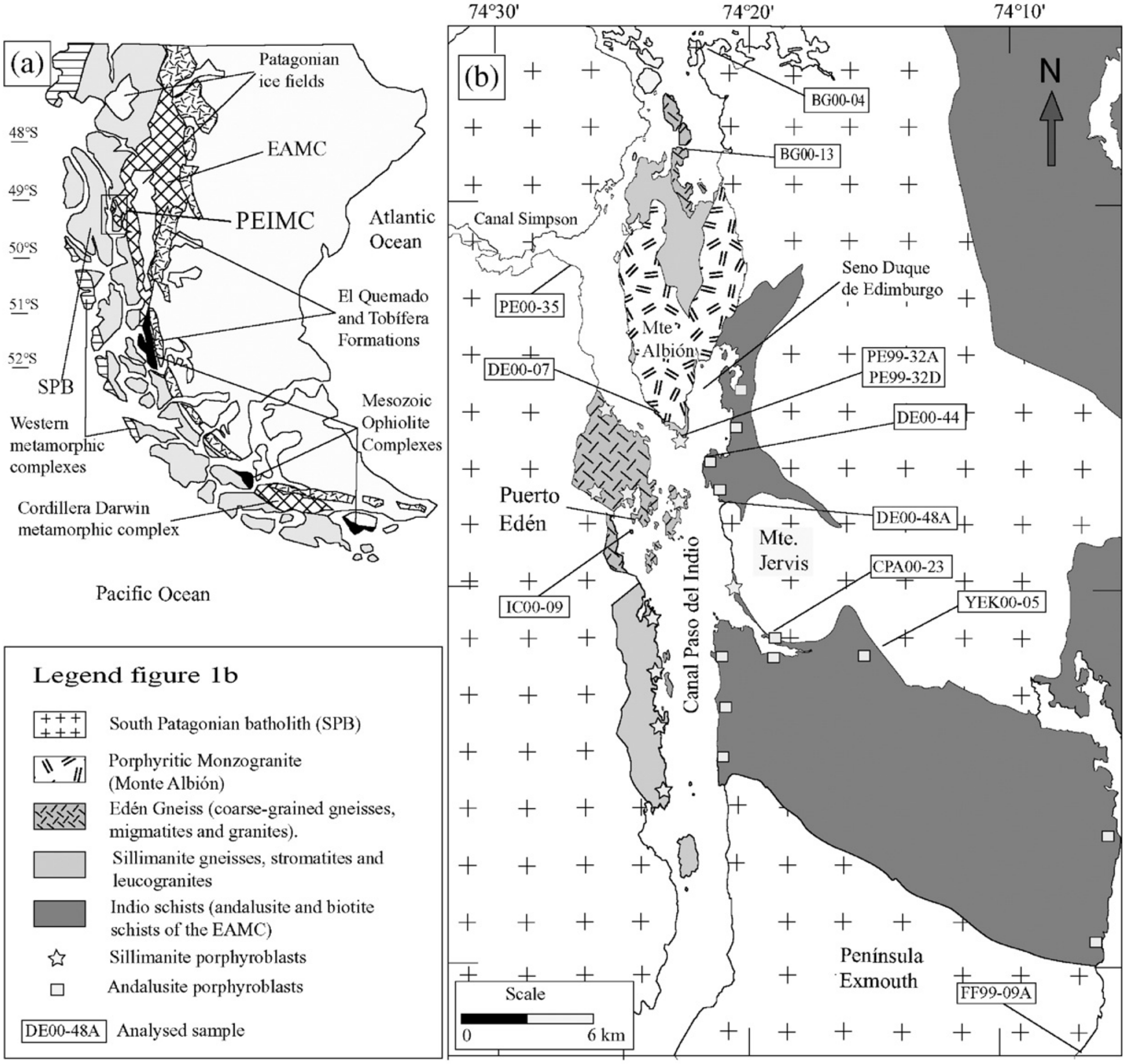

Fig. 1. (a) Location map of the southwestern Patagonian geological units (modified from Pankhurst et al., 1998). Eastern belt of metamorphic rocks are the Eastern Andean Metamorphic Complex (EAMC) and the Cordillera Darwin metamorphic complex; South Patagonian Batholith (SPB); Puerto Edén Igneous and Metamorphic Complex (PEIMC); Mesozoic ophiolite complexes (Late Jurassic–Early Cretaceous), oceanic-type mafic floor remnants of the Rocas Verdes basin. (b) Geological map of the PEIMC and surrounded areas (modified from Watters, 1964). Localities and studied samples are indicated.

after loss of the fractionated liquid (e.g. Milord et al., 2001). The mesosome comprises refractory material that may or may not included in peritectic reactions. The mesosome could coexist with unsegregated melt, both being affected by partial back reactions and give rise to the melanosome (Kriegsman, 2001).

Migmatites are subdivided into metatexites and diatexites. *Metatexite* is a migmatite with discrete leucosomes, mesosomes and melanosomes (Wimmenauer and Bryhni, 2002) containing pre-migmatisation layers, foliation or banding, which are not obliterated by partial melting (Brown, 1973). The initial nearly single-stage

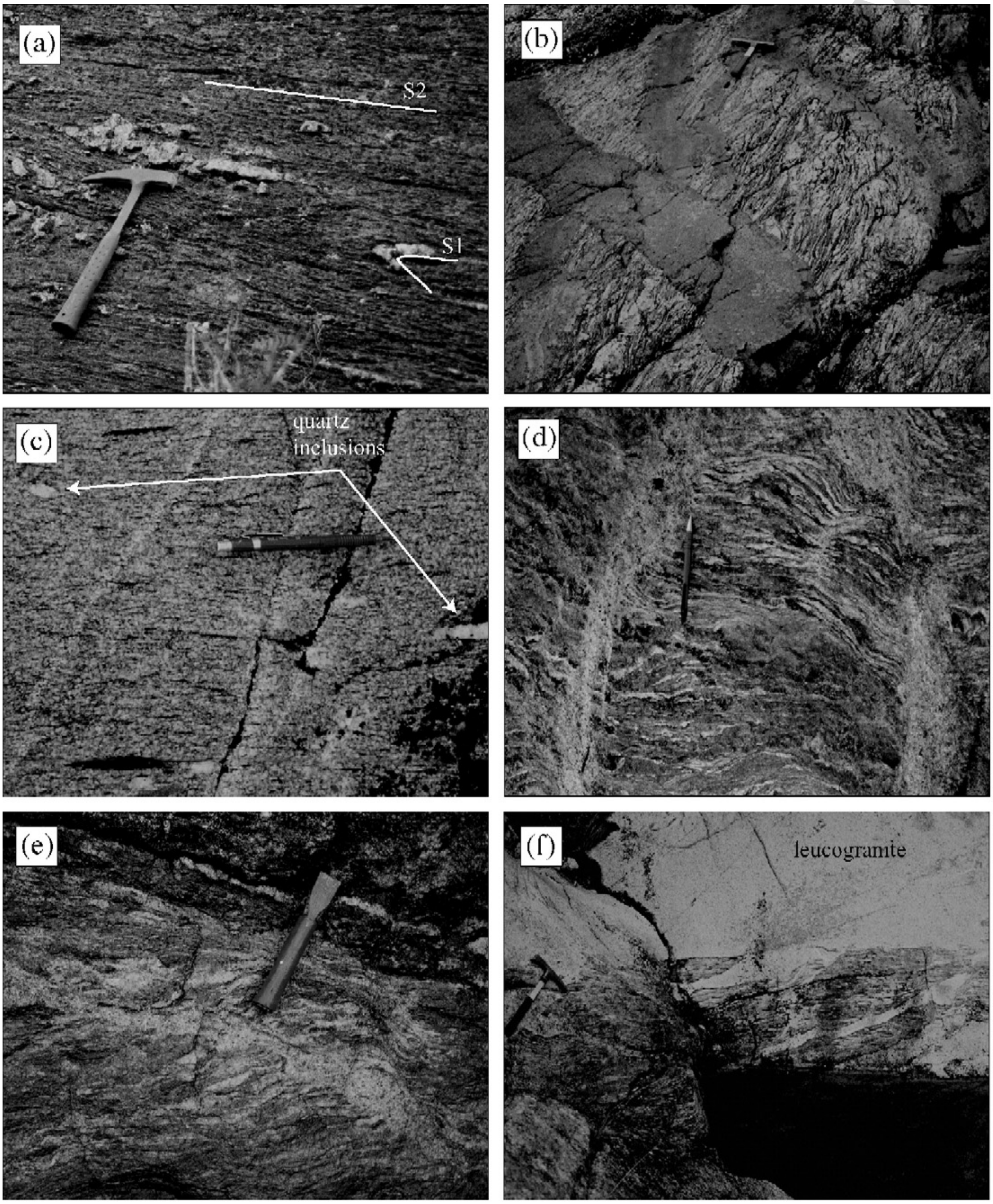

Fig. 2. (a) Andalusite schist with folded and boudinaged quartz bands in S_2 transposing main foliation. (b) Sillimanite gneisses with anastomosing S_2 foliation. Mafic dykes with fine-grained (chilled) margins. (c) Coarse-grained gneiss with oriented schlieren of biotite–sillimanite and ellipsoidal quartz inclusions. (d) and (e) migmatites (stromatites) with leucosome located in interpreted S–C type structures. (f) Sillimanite gneisses and/or stromatites intruded by leucogranite network.

process known as the metatexite model produces leucocratic, residuum-free granites (e.g. Sawyer, 1998; and references therein). *Diatexite* is a variety of migmatite where darker and lighter parts form schlieren and nebulitic structures which merge into one another (Wimmenauer and Bryhni, 2002). Pre-migmatisation structures are destroyed and homogenization and coarsening of the textures occurred (Brown, 1973; Sawyer, 1998; Milord et al., 2001). The melt fraction in migmatites can be increased by: (1) a rise of metamorphic temperature (Brown, 1973); (2) melt injection from elsewhere (Greenfield et al., 1996); or (3) melt redistribution within melt layers (Sawyer, 1998). The multi-stage process, known as the diatexite model, can produce residuum-rich granites (e.g. Sawyer, 1998). Diatexites with high and low melt fraction are respectively called leucodiatexite and melanodiatexite.

The Puerto Edén igneous and metamorphic complex (PEIMC) is an exceptional N–S trending narrow belt of medium- to high-grade metasedimentary rocks, migmatites and plutonic rocks enveloped by biotite–hornblende plutons within the eastern margin of the South Patagonian batholith (49°S; Fig. 1). Metamorphic overgrowth zones of zircon from a sillimanite paragneiss record a Late Jurassic age of ~ 150 Ma (SHRIMP U–Pb zircon; Hervé et al., 2003), taken as evidence of local gneiss formation under in situ anatectic conditions by the emplacement of Jurassic plutonic rocks of the SPB. This paper examines the mineral, geochemical and isotopic variations among a suite of rocks from the PEIMC with the aim of evaluating the relationship between the anatexis of metapelites and the generation of crustal granitic melts coeval with both the formation of the earliest batholithic components and the development of the Rocas Verdes marginal basin along the south-western continental margin of Gondwana.

2. Analytical methods

Mineral compositions were determined at Universität Stuttgart using a CAMECA SX-100 microprobe under operating conditions of 15 kV and 15 nA. We applied either a wide beam of 7–10 μm (micas and feldspars) or a focused beam (garnet and amphiboles). Counting times per element on the peak and as on the background were 20 s each. The standards used were natural wollastonite (Si, Ca), natural orthoclase (K), natural albite (Na), natural rhodonite (Mn), synthetic Cr_2O_3 (Cr), synthetic TiO_2 (Ti), natural hematite (Fe), natural barite (Ba), synthetic MgO (Mg), synthetic Al_2O_3 (Al) and synthetic NiO (Ni).

Rock samples for geochemical and isotopic analyses consisted of 1–3 kg of material, which were crushed and split to 200 g, and then pulverised in an agate mill. Bulk-rock analyses for major and trace elements were performed at Universidad de Chile using a Perkin Elmer Sequential P400 ICP-AES. Major element oxides (Si, Ti, Al, Fe, Mn, Mg, Ca, Na and K), Cr and Zr were measured after fusion with ($Li_2B_4O_7+2Na_2CO_3$). FeO was volumetrically determined after the reduction–oxidation reaction with $K_2Cr_2O_7$. Trace elements (REE, Y, Sc and Hf) were concentrated by ion exchange using AG50WX8 resin. Nb and Th were determined after NaOH fusion and Al elimination. Loss on ignition was measured after heating to 950 °C in a porcelain crucible.

Rb–Sr and Sm–Nd isotope analyses were performed at Universidade de São Paulo, except sample FF99-09 (NERC Isotope Geosciences Laboratory, Keyworth, U.K.). Rb and Sr contents were determined by X-ray fluorescence spectrometry, and $^{87}Sr/^{86}Sr$ ratios measured by thermal ionization mass-spectrometry, corrected for mass fractionation to $^{86}Sr/^{88}Sr=0.1194$ normalization. Sm and Nd (and other lanthanides) were chemically separated on HDEHP supported on teflon powder columns. The Sm and Nd concentrations were obtained by isotopic dilution using a mixed ^{149}Sm and ^{150}Nd tracer. All radiogenic isotopes analyses were performed using a VG 354 Micromass spectrometer. The isotopic ratios were calculated relative to $^{146}Nd/^{144}Nd=0.7219$. At the time of the analyses the following standard values were obtained: $^{87}Sr/^{86}Sr=0.71026\pm0.00002$ (2σ) for NBS-987 and $^{143}Nd/^{144}Nd=0.511847\pm0.00002$ (2σ) and 0.512662 ± 0.000027 (2σ) values for La Jolla and BCR-1 respectively.

3. Regional geological background

The Eastern Andean Metamorphic Complex (EAMC; Hervé, 1993), considered as the metamorphic basement of the southern Patagonian Andes (Fig. 1a; 48°–52°S), is mainly composed of a poly-deformed assemblage of metapelites, metapsammites, metagreywackes and marbles, as well as local metabasites. The turbiditic protoliths, deposited along a passive continental margin (Faúndez et al., 2002; Augustsson and Bahlburg, 2003), has a maximum sedimentation age of 374 Ma at ca. 48°S (Thomson and Hervé, 2002). This succession underwent greenschist facies regional metamorphism (e.g. Ramírez, 2003; Hervé et al., 1998) probably at 300±23 Ma (Thomson et al., 2000). The intrusion of large volumes of basaltic and tonalitic melts caused Late Jurassic high-temperature low-pressure metamorphism (amphibolite facies) superimposing on the otherwise low-grade metamorphic EAMC rocks along the eastern contact of the South Patagonian batholith (Calderón and Hervé, 2000; Calderón, 2005).

Plutonic activity in the South Patagonian batholith (SPB) ranges from 151 to 16 Ma (Bruce et al., 1991;

Martin et al., 2001). The oldest plutons occur on the eastern margin (ca. 151–141 Ma), with earliest Cretaceous units in the west (ca. 137 Ma), and Late-Cretaceous to Cenozoic granitoids concentrated near the central axis of the batholith (U–Pb conventional and SHRIMP zircon ages; Martin et al., 2001). The SPB has calc-alkaline affinities and is divided into a tonalitic and a granodioritic series, suggesting that differentiation of two distinct parental magmas occurred during batholith formation (Nelson et al., 1988; Weaver et al., 1990). Sr, Nd and Pb isotope data of rocks at 48°S have been interpreted to show that contamination by Palaeozoic metasedimentary rocks played an important role in the petrologic and chemical evolution of the batholith which is composed of mixtures of mantle-derived magmas and crustal components with a progressive decrease in crustal involvement with time (Weaver et al., 1990).

Volcano-sedimentary successions of the El Quemado and the Tobífera Formations (Fig. 1a), with dominant rhyolitic pyroclastic rocks, represent the westernmost components of the Jurassic Chon Aike silicic Large Igneous Province (Pankhurst et al., 1998). Crystallisation ages of 156–153 Ma have been reported for El Quemado Formation (Pankhurst et al., 2000) and of ca. 149 Ma for the Tobífera Formation (Calderón, 2006). A subaquatic depositional environment has been proposed for at least part of the Tobífera Formation (Hanson and Wilson, 1993), preceding the formation of the Late Jurassic to Early Cretaceous oceanic-type mafic floor of the Rocas Verdes marginal basin (Dalziel, 1981; Stern et al., 1992; Mukasa and Dalziel, 1996). However, a plagiogranite from the northernmost remnant of the Rocas Verdes basin (Sarmiento Ophiolite Complex), dated at 150 Ma (Calderón, 2006), indicate that the formation of the oceanic-type igneous crust was coeval with the deposition of the Tobífera Formation.

4. Puerto Edén igneous and metamorphic complex

The foliated rocks in Puerto Edén (Fig. 2) were subdivided by Watters (1964) in two metamorphic domains: the Indio schists, comprising biotite–white mica–plagioclase–quartz and biotite–white mica–staurolite–andalusite–cordierite–plagioclase–quartz fine- to medium-grained schists and gneisses (all with tourmaline, graphite, zircon, apatite, corundum and Fe–Ti oxides as accessory phases); and the Edén gneiss, comprising biotite–white mica–sillimanite–cordierite–plagioclase–K-feldspar–quartz gneisses and inhomogeneous medium- and coarse-grained gneisses with narrow and elongated quartz-rich inclusions and schlieren of biotite and sillimanite (Fig. 2c). Foliated plutonic rocks such as garnet–tourmaline, biotite–garnet leucogranites and felsic pegmatites are spatially related with sillimanite gneisses. Although the boundary between both domains is hidden by the Canal Paso del Indio, in some islands the exposure of a transitional zone is likely, marked by “permeation” sillimanite gneisses showing small acid lenses and veins parallel to the gneissic layering (Watters, 1964). The cited features of permeation rocks coincide with the description of structural elements of some migmatites, which were observed along the western coast of the channel (stromatites and nebulites in the Edén gneiss) and to the north of Monte Albión (Fig. 1).

The kilometre-sized and N–S trending Monte Albión composite pluton, is mainly composed of biotite schlieren-bearing porphyritic monzogranite with accessory garnet discernable along the shore line. Decimetre-wide, amphibolitised dismembered (synplutonic) mafic dykes occur within this pluton and also in some migmatites and leucogranites. Strongly foliated amphibole- and biotite-bearing metabasites crop out in the Indio schists and Edén gneiss and are interpreted as mafic dykes preceding

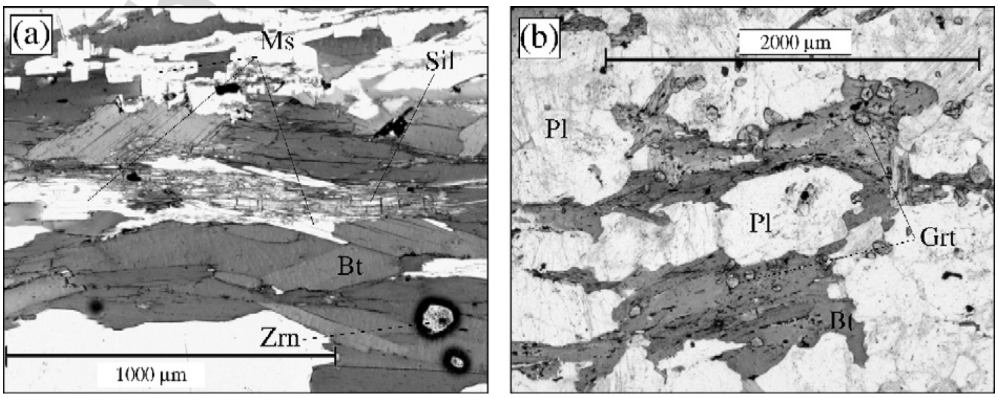

Fig. 3. Photomicrographs. (a) Schlieren in coarse-grained gneiss with biotite and sillimanite as precursors of retrograde white mica. (b) Millimetre-sized leucosome in sillimanite gneisses. The biotite, plagioclase and garnet composition were used for geothermobarometric calculations.

the high-grade metamorphism (Watters, 1964; Calderón, 2005). The Indio schists, the Edén gneiss and the Monte Albión composite pluton, grouped in the PEIMC, are intruded by undeformed mafic dykes, most of them with chilled margins. The PEIMC is flanked on the east and west by biotite–hornblende granitoid plutons, weakly foliated at their margins.

5. Metamorphism and structures

The mineral assemblages in andalusite schists (biotite + plagioclase + andalusite + tourmaline ± cordierite ± corundum), where staurolite occur as minor and anhedral/relic inclusions in andalusite porphyroblasts, and sillimanite gneisses (biotite + plagioclase + sillimanite ± K-

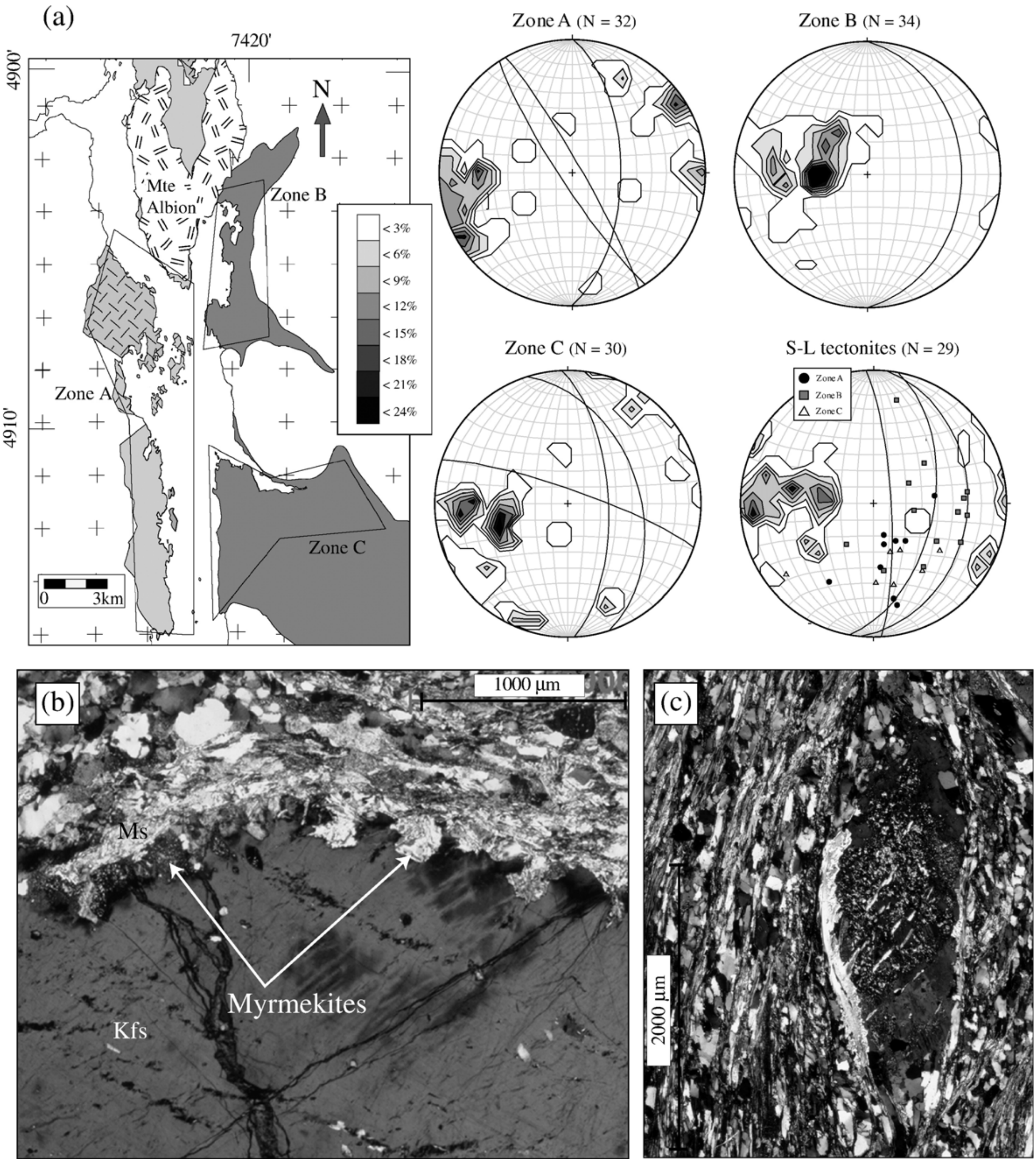

Fig. 4. (a) Contour diagrams (lower hemisphere) of main foliation planes and S–L tectonites in three zones of the PEIMC. Greyscale indicates the concentration of poles of foliation. It is plotted the plane associated with the high density of poles. (b) and (c) are photomicrographs of a granite mylonite. (b) K-feldspar porphyroclast with lobes of myrmekite retrogressed to very fine-grained white mica. (c) S–C type microstructure in dynamically recrystallised matrix and plagioclase porphyroclast with σ-type and quarter mats microstructures indicating dextral (reverse) shear sense.

feldspar ± cordierite ± corundum), indicate their crystallisation under high-temperature–low-pressure conditions of metamorphism. The widespread presence of biotite in schists, gneisses and migmatites is the result of chlorite + muscovite (greenschist facies) decomposition reactions. Retrograde white mica has overgrown andalusite and biotite in schists and was formed at the expense of biotite and sillimanite in gneisses (Fig. 3). The pinnitisation of cordierite, the chloritisation of biotite and the crystallisation of prehnite in veins and on biotite cleavage planes, are characteristic features of retrograde metamorphism.

Andalusite schists and sillimanite gneisses show the earliest S_1 foliation preserved in tight folds of centimetre-sized quartz bands (Fig. 2a) and in microlithons of a steeply dipping and anastomosing S_2 crenulation or shear band cleavage (Fig. 2b). The S_2 composite foliation consists of a NW–SE trending and moderate to steep north-dipping foliation, and a N–S trending and steeply to moderately east-dipping foliation with variable south- and east-plunging white mica mineral lineations (Fig. 4a). The latter is dominant along both shores of the N–S trending Canal Paso del Indio and the Seno Duque de Edimburgo (Fig. 1). In the Edén gneiss, foliated decametre-sized sheets of quartzofeldspathic coarse-grained gneisses contain schlieren of biotite and sillimanite subparallel to the S_2 foliation. Oriented centimetre-long ellipsoidal quartz-rich inclusions, in some cases tightly folded bands, are abundant in these rocks as well (Fig. 2c). Microstructures such as quartz strain-shadows around blasts of plagioclase and andalusite, with biotite at inter-boudin domains, and the undulose extinction of some andalusite porphyroblasts indicate S_2-related deformation processes which have acted late or after the peak metamorphic crystallisation. This late deformation is also discernable in the foliated leucogranite dykes in the Edén gneiss.

Several N–S trending narrow mylonites (~ 1–3 m wide) crosscut the Edén gneiss and the eastern side of the Monte Albión composite pluton. The mylonites have formed in coarse-grained gneisses dipping to the east with east-plunging mineral and stretching lineations defined by syntectonic white mica and quartz strain-shadows. Myrmekite around K-feldspar porphyroclasts (Fig. 4b) look similar to those described by Simpson and Wintsch (1989). These authors interpreted these symplectites in as being stress-controlled. Thus, we think that they formed at temperatures of at least 400–500 °C during dynamic recrystallisation (cf. Passchier and Trouw, 1996). Microstructures, such as σ-type plagioclase porphyroclasts, strain shadows, quarter mats and S–C shear bands, indicate a west-vergent sense of shear displacement (Fig. 4c).

6. Petrography of the chemically analysed samples

Andalusite schist (DE00-44 and W107) and sillimanite gneiss (PE99-32A) are fine-grained rocks that contain muscovite and reddish brown biotite in anastomosing lepidoblastic domains, and quartz–plagioclase granoblastic bands. Although the plagioclase (An_{15-20}) is the dominant feldspar in both rocks, the sillimanite gneiss also contains small amounts of K-feldspar. Biotite contains zircon inclusions 0.01–0.2 mm in size. Anhedral tourmaline, apatite, graphite and Fe–Ti oxides are accessory phases. Some sillimanite gneisses that crop out near the analysed sample have microscopic plagioclase–biotite–garnet bearing leucosome bands.

Migmatite (BG00-13) generally preserves some schistose or gneissic structures resulting from variable proportions of melanosome and leucosome bands (Fig. 2e). The melanosome is formed by abundant biotite and a significantly greater proportion of accessory phases (e.g. zircon, Fe–Ti oxides). Biotite is retrogressed to chlorite and white mica, both with decussate texture. The leucosome bands are rich in quartz and plagioclase (An_{12-30}). Accessory phases are muscovite, apatite, tourmaline, K-

Table 1
Summary of compositions of plagioclase and garnet in the analysed samples

Lithology	Sample	Plagioclase	Garnet
Andalusite schist	W107	An_{15-20}	–
Sillimanite gneiss	PE99-32A	An_{15-20}	–
Leucosome (in sillimanite gneiss)	DE00-13	An_{25-35}	Alm_{63-65} $Spess_{27-32}$ $Py_{3-5}Gross_{2-3}$
Leucosome (in migmatite)	BG00-13	An_{12-30}– An_{1-3}	–
Grt–Tur leucogranite	PE99-32D	An_{0-2}	Alm_{67-72} $Spess_{25-30}$ $Py_{2-3}Gross_{0-1}$
Grt–Bt leucogranite	PE00-13	An_{18-25}	Alm_{74-76} $Spess_{19-22}Py_3$ $Gross_{2-3}$
Ms–Grt leucogranite	DE0048A	An_{2-16}	Alm_{70-72} $Spess_{26}Py_2$ $Gross_{1-2}$
Coarse-grained gneiss	IC00-09	An_{24-35}	–
Synplutonic dyke	BG00-12	–	Alm_{72-76} $Spess_{11-17}$ $Py_{3-6}Gross_{7-9}$
Porphyritic monzogranite	DE00-07	An_{25-33}– An_{1-1}	–
Biotite–garnet porphyritic monzogranite	DE00-16	An_{17-23}– An_{1-10}	Alm_{67-78} $Spess_{18-30}Py_{1-2}$ $Gross_{1-3}$
Bt–Hbl–(Aln) granodiorite	YEK00-05	An_{4-52}	–

feldspar and garnet. The latter phase appears only as pseudomorphs. Plagioclase aggregates delimited by thin lepidoblastic bands are a common feature of these domains.

Coarse-grained gneiss (IC00-09) consists of an allotriomorphic granitic quartzo-feldspathic assemblage (90–95%; Fig. 2c) with oriented biotite–sillimanite bearing schlieren (5–10%). The K-feldspar exhibits poikilitic texture defined by euhedral plagioclase (An_{24-35}) inclusions. The schlieren domains are composed of reddish brown biotite (with zircon inclusions of 0.05–1.5 mm in size), minor fibrolite, K-feldspar and retrograde muscovite. Noticeable are the microscopic similarities between the aggregates of biotite and sillimanite of these rocks and the lepidoblastic domains in the sillimanite gneisses.

Porphyritic monzogranite (DE00-07 and DE00-16) contains K-feldspar megacrysts (1–4 cm long) showing both myrmekitic and perthitic textures. K-feldspar is poikilitic containing biotite, subhedral plagioclase and apatite inclusions. Plagioclase (An_{25-33} and also late formed An_{1-10}) is anhedral (sizes between 0.5 and 4 mm) with oscillatory zoning. It is slightly sericitised and commonly forms cumulates delimited by thin quartz bands. Biotite, isolated or grouped in schlieren of ca. 3 cm long (~ 3% of whole rock), is reddish brown and slightly chloritised.

Biotite granite (FF99-09A), which crops out in the eastern side of the Península Exmouth (Fig. 1), is medium-grained, allotriomorphic, and mainly composed of quartz forming an inequigranular mosaic (locally showing triple junctions). Subhedral plagioclase shows oscillatory zoning, polysynthetic twinning, and minor sericite alteration. K-feldspar is an anhedral perthitic phase exhibiting poikilitic texture (with subhedral plagioclase inclusions). Some K-feldspar phenocrysts are also present. The mafic component is reddish brown anhedral biotite (1–4 mm, less than 5%), that contains minor zircon and apatite inclusions.

Garnet and tourmaline leucogranite (PE99-32D) is a fine-to medium-grained hypidiomorphic rock, composed of an irregular aggregate of quartz with undulose extinction, myrmekitic and anhedral plagioclase (An_{0-2}), and microperthitic microcline. Garnet and tourmaline are

Table 2a
Representative chemical analyses of white mica

Sample	W107				PE9932A		IC0009		DE0048A	
lithology	Andalusite schist				Sillimanite gneiss		Coarse-grained gneiss		Grt–Ms leucogranite	
Oxides (wt.%)										
SiO_2	45.47	46.01	50.26	51.61	44.33	44.93	44.99	45.08	44.31	44.51
Al_2O_3	37.49	36.75	33.27	32.78	36.99	36.25	35.56	37.34	36.53	36.60
TiO_2	0.11	0.72	0.36	0.32	0.43	0.53	1.10	0.95	0.06	0.05
FeO	0.79	0.96	0.97	0.66	1.12	1.08	1.15	0.99	1.75	1.80
MnO	0.04	0.00	0.02	0.03	0.00	0.02	0.00	0.01	0.02	0.02
MgO	0.30	0.40	0.38	0.27	0.46	0.43	0.53	0.42	0.28	0.27
CaO	0.07	0.03	1.04	1.31	0.02	0.02	0.04	0.02	0.00	0.01
Na_2O	1.02	1.16	3.23	3.54	1.27	1.17	0.53	0.55	0.89	0.95
K_2O	9.77	9.57	7.35	6.85	9.70	9.87	10.72	10.50	10.35	10.53
Sum	95.06	95.60	96.87	97.36	94.32	94.29	94.61	95.85	94.20	94.73
Cations										
Si	3.02	3.04	3.25	3.30	2.98	3.02	3.02	2.98	3.00	3.00
AlIV	0.98	0.96	0.75	0.70	1.02	0.98	0.98	1.02	1.00	1.00
Sum	4	4	4	4	4	4	4	4	4	4
AlVI	1.95	1.89	1.78	1.78	1.91	1.89	1.84	1.89	1.91	1.90
Ti	0.01	0.04	0.02	0.02	0.02	0.03	0.06	0.05	0.00	0.00
Fe	0.04	0.05	0.05	0.04	0.06	0.06	0.06	0.05	0.10	0.10
Mn	0.00	0.00	0.00	0.00	0.00	0.00	0.00	0.00	0.00	0.00
Mg	0.03	0.04	0.04	0.03	0.05	0.04	0.05	0.04	0.03	0.03
Sum	2.03	2.02	1.89	1.85	2.04	2.02	2.02	2.04	2.04	2.03
Ca	0.01	0.00	0.07	0.09	0.00	0.00	0.00	0.00	0.00	0.00
Na	0.13	0.15	0.40	0.44	0.16	0.15	0.07	0.07	0.12	0.12
K	0.83	0.81	0.61	0.56	0.83	0.85	0.92	0.89	0.89	0.90
Sum	0.96	0.96	1.08	1.09	1.00	1.00	0.99	0.96	1.01	1.03
# Mg	0.40	0.43	0.41	0.42	0.42	0.42	0.45	0.43	0.22	0.21

Mineral formula based on 11 oxygens.

subhedral with sizes between 3 and 7 mm. The intergrowths of muscovite flakes and microcrystalline quartz are interpreted as late crystallisation phases that define millimetre-sized shear bands. Leucogranites form decimetre-wide tabular bodies intruding sillimanite gneisses that in some cases contain garnet and biotite (PE0013).

Muscovite and garnet leucogranite (DE00-48A) is an isotropic and medium grained rock composed of anhedral quartz with undulose extinction, subhedral plagioclase (An_{2-16}) with oscillatory zoning, and microperthitic K-feldspar (microcline) with plagioclase inclusions. Muscovite (<2 mm) displays discrete kink bands. Garnet (<0.3 mm) is a minor accessory phase. Leucogranite DE00-48A is a tabular body (2 m thick), that cross-cuts an andalusite schist and an undeformed mafic dyke within the schists.

Biotite–hornblende–allanite granodiorites and tonalites (YEK00-05, BG00-04, CPA00-23 and PE00-35) are medium-grained isotropic bodies with hypidiomorphic–allotriomorphic textures. Quartz is anhedral and has undulose extinction. Subhedral plagioclase (An_{4-52}; zoned crystals with calcic cores and more sodic rims) is slightly sericitised. Microcline feldspars in granodiorites are anhedral and have poikilitic texture with subhedral plagioclase and amphibole inclusions. Euhedral and zoned allanite shows narrow rims of colourless epidote. Hornblende and biotite show low- to medium degrees of alteration to chlorite. Sample YEK00-05 shows the least degree of alteration.

7. Mineral compositions

Mineral compositions in schists, gneisses, migmatites and plutonic rocks were determined by electron microprobe (CAMECA SX-100) analyses of ca. 20 grains per thin section. Garnet and plagioclase compositions are summarized in Table 1. Representative chemical analyses of muscovite and biotite are presented in Tables 2a and 2b.

Table 2b
Representative chemical analysis of biotite

Sample	W107		PE9932A		IC0009		DE0007		YEK0005	
lithology	Andalusite schist		Sillimanite gneiss		Coarse-grained gneiss		Porphyritic monzogranite		Bt–Hbl–(Aln) granodiorite	
Oxides (wt.%)										
SiO_2	33.57	33.50	33.55	33.79	33.78	33.78	33.51	33.35	34.88	35.32
TiO_2	1.65	2.51	2.22	2.53	3.37	3.09	2.79	2.58	3.20	3.55
Al_2O_3	20.39	21.32	19.24	19.61	19.38	18.79	18.30	18.08	14.74	14.29
Cr_2O_3	0.04	0.07	0.06	0.05	0.04	0.03	0.02	0.00	0.00	0.03
FeO	21.17	22.02	22.30	21.50	23.46	23.17	26.94	27.40	23.67	22.82
MnO	0.23	0.26	0.19	0.18	0.37	0.38	0.40	0.46	0.75	0.69
MgO	8.17	6.83	7.79	7.97	6.20	6.42	4.61	4.77	8.62	9.27
CaO	0.08	0.04	0.08	0.09	0.04	0.07	0.06	0.02	0.04	0.07
Na_2O	0.19	0.24	0.26	0.36	0.14	0.10	0.14	0.13	0.04	0.08
K_2O	8.90	8.43	8.82	8.84	9.64	9.73	9.46	9.62	9.25	9.50
Sum	94.40	95.21	94.50	94.93	96.41	95.56	96.23	96.41	95.19	95.63
Cations										
Si	5.21	5.15	5.24	5.23	5.22	5.27	5.28	5.27	5.49	5.51
AlIV	2.79	2.85	2.76	2.77	2.78	2.73	2.72	2.73	2.51	2.49
Sum	8.00	8.00	8.00	8.00	8.00	8.00	8.00	8.00	8.00	8.00
AlVI	0.94	1.02	0.78	0.80	0.75	0.72	0.68	0.64	0.22	0.14
Ti	0.19	0.29	0.26	0.29	0.39	0.36	0.33	0.31	0.38	0.42
Cr	0.01	0.01	0.01	0.01	0.00	0.00	0.00	0.00	0.00	0.00
Fe	2.75	2.83	2.91	2.78	3.03	3.02	3.55	3.62	3.11	2.98
Mn	0.03	0.03	0.02	0.02	0.05	0.05	0.05	0.06	0.10	0.09
Mg	1.89	1.57	1.81	1.84	1.43	1.49	1.08	1.12	2.02	2.16
Sum	5.81	5.75	5.80	5.75	5.65	5.65	5.70	5.75	5.83	5.79
Ca	0.01	0.01	0.01	0.01	0.01	0.01	0.01	0.00	0.01	0.01
Na	0.06	0.07	0.08	0.11	0.04	0.03	0.04	0.04	0.01	0.02
K	1.76	1.65	1.76	1.75	1.90	1.93	1.90	1.94	1.86	1.89
Sum	1.83	1.73	1.85	1.87	1.95	1.98	1.96	1.98	1.88	1.93
# Mg	40.76	35.62	38.39	39.79	32.02	33.06	23.36	23.69	39.36	42.01

Mineral formula based on 22 oxygens.

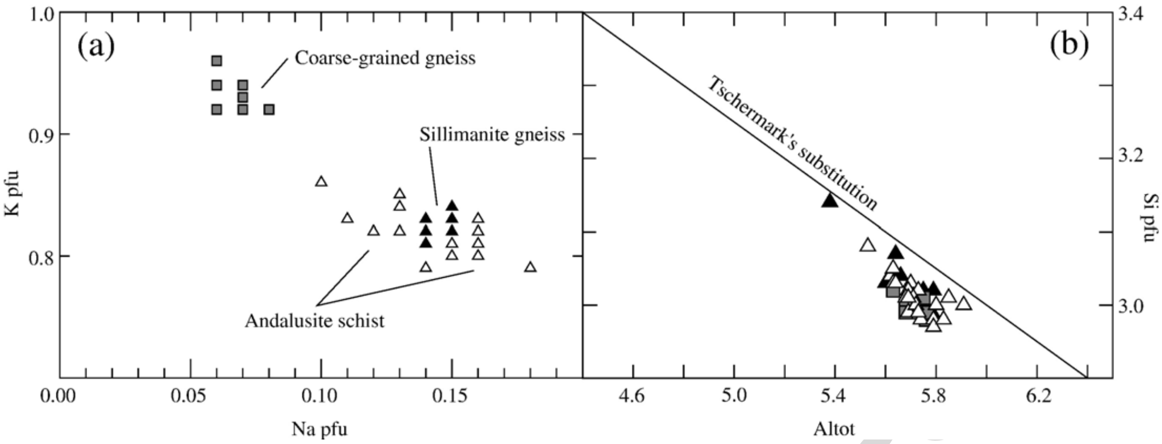

Fig. 5. (a) K–Na and (b) Si–Al variation of white mica from schist and gneisses.

The mean Mg/(Mg+Fe) ratio of reddish brown biotite from metamorphic rocks and biotite granitoids is 0.40 (andalusite schist), 0.39 (sillimanite gneiss), 0.32 (coarse-grained gneiss), 0.25 (garnet leucogranite), 0.22 (porphyritic monzogranite) and 0.18 (garnet porphyritic granite). The greenish brown biotite of the biotite–hornblende–allanite granodiorite shows a Mg/(Mg+Fe) ratio of 0.40. In general, the Al contents of the reddish brown biotites are more or less constant (3.4–3.9 per formula unit=pfu, based on 22 oxygens) and higher than those of the greenish brown biotite (2.6–2.7 pfu) which crystallised co-magmatically with hornblende.

The titanium content of biotite, expressed as Ti pfu, shows a progressive increase with metamorphic grade from

Table 3
Composition of biotite, garnet and plagioclase in leucosome used in thermobarometric calculations

Mineral analysis no.	Biotite				Garnet				Plagioclase			
	1	2	3	4	1	2	3	4	1	2	3	4
Oxides (wt.%)												
SiO_2	33.74	34.60	34.14	33.25	37.20	36.88	37.49	37.24	59.24	59.84	59.88	60.78
TiO_2	3.15	3.31	3.15	3.23	0.07	0.04	0.07	0.04	0.02	0.02	0.01	0.02
Al_2O_3	19.55	19.84	19.46	20.01	20.73	20.90	20.43	21.01	25.51	24.89	24.44	24.14
Cr_2O_3	0.05	0.06	0.05	0.06	0.02	0.02	0.03	0.02	0.01	0.01	0.01	0.01
FeO	21.44	20.50	21.10	21.00	28.59	27.89	28.32	28.53	0.05	0.01	0.05	0.10
MgO	7.57	7.12	7.53	7.22	1.99	1.79	1.81	1.93	0.04	0.01	0.00	0.03
MnO	0.39	0.32	0.33	0.43	12.30	12.11	12.18	12.18	0.00	0.03	0.04	0.04
Na_2O	0.16	0.18	0.15	0.12	0.00	0.03	0.04	0.03	7.83	8.31	8.24	8.50
K_2O	9.01	9.34	8.97	9.02	0.00	0.04	0.05	0.03	0.19	0.21	0.20	0.21
CaO	0.04	0.05	0.06	0.04	1.15	0.99	1.05	1.03	6.94	6.17	5.90	5.48
BaO	0.23	0.30	0.30	0.28	0.03	0.04	0.00	0.00	0.02	0.02	0.05	0.03
NiO	0.01	0.10	0.00	0.03	0.00	0.03	0.03	0.00	0.04	0.03	0.06	0.00
H_2O	4.68	4.29	4.77	5.33	0.00	0.00	0.00	0.00	0.12	0.46	1.10	0.68
Total	100.00	100.00	100.00	100.00	102.07	100.77	101.49	102.04	100.00	100.00	100.00	100.00
Cations												
Si	2.61	2.65	2.64	2.59	2.97	2.99	3.02	2.97	2.65	2.68	2.70	2.72
Ti	0.18	0.19	0.18	0.19								
Al	1.79	1.79	1.77	1.84	1.95	1.99	1.94	1.98	1.34	1.31	1.30	1.27
Fe	1.39	1.31	1.36	1.37	1.91	1.89	1.91	1.91				
Mg	0.87	0.81	0.87	0.84	0.24	0.22	0.22	0.23				
Mn	0.03	0.02	0.02	0.03	0.83	0.83	0.83	0.82				
Na	0.02	0.03	0.02	0.02					0.68	0.72	0.72	0.74
K	0.89	0.91	0.88	0.90					0.01	0.01	0.01	0.01
Ca					0.10	0.09	0.09	0.09	0.33	0.30	0.28	0.26
Sum	7.77	7.73	7.75	7.76	8.00	8.00	8.00	8.00	5.02	5.02	5.01	5.01

Mineral formula based in 12 oxygens (Bt), 8 cations (Grt) and 8 oxygens (Pl).

the andalusite schists to sillimanite medium- to coarse-grained gneisses (0.25 to 0.36 pfu). In biotite granites the Ti contents of biotite yielded variable mean values: biotite–garnet leucogranite (0.28), porphyritic monzogranite (0.30) and porphyritic biotite–garnet monzogranite (0.261). Biotite in biotite–hornblende–allanite granodiorite has the highest value of Ti (0.42).

Muscovites from schists, gneisses and coarse-grained gneisses have Si contents of 3.0 to 3.1 pfu (based on 11 oxygens). Muscovites in the andalusite schist and sillimanite gneiss show variable contents of K and Na, contrasting with the K-rich composition in the coarse-grained gneiss (Fig. 5a). White mica compositions are close to the ideal Tschermak's substitution line (Fig. 5b), indicating the lack of ferric muscovite component.

7.1. P–T estimates

Temperatures obtained from garnet–biotite pairs and GASP pressures were estimated from compositions of garnets (50 to 100 μm; Fig. 3b) included within biotite selvedges in a millimetre-sized plagioclase-bearing leucosome in a sillimanite gneiss using the calibrations of Holdaway (2000, 2001). The low content of ferric-iron in biotite and muscovite in schists and gneisses and the ubiquitous presence of graphite (cf. Labotka, 1991) indicate low oxidation conditions (QFM buffer) in the course of migmatisation, favourable for geothermobarometric calculations. As the high Ti and Mn contents in biotite and garnet (Table 3), respectively, are outside the range optimal for geothermometry, a temperature error of ± 50 °C is considered (commonly ±25 °C; Holdaway, e-mail communication). Garnet with 4–5% of grossular content and plagioclase with 24–35% of anorthite, allow the use of the GASP geobarometer. Although the sillimanite is in the rock but nowhere in direct contact with garnet and biotite, we assumed equilibrium of these phases. Nevertheless, the resulting pressures are upper pressure limits. The GASP geobarometer has an absolute error of ±0.8 kbar considering a temperature error of ±25 °C, therefore due to the higher temperature error an error of ±1 kbar is considered.

Considering 11.6% and 3% of total iron as Fe^{3+} content in biotite and garnet respectively (recommended values by Holdaway, 2000), the calculated temperature and pressure conditions for eight mineral assemblages are 620 to 640 °C (±50 °C) and of 3 to 3.3 kbar (±1 kbar). Considering lower Fe^{+3} contents in biotite and garnet, slightly higher pressure and temperature conditions would result.

High-grade metamorphism occurred below 4.5 kbar (according to the Al_2SiO_5 triple point of Pattison, 1992) as indicated by the widespread occurrence of andalusite in the schists. In terrains with sillimanite gneisses and migmatites, partial melting or migmatisation was estimated to occur above the intersection of the muscovite dehydration-melting reaction and the solidus for the minimum granite composition (IP1; see Fig. 6). According to the phase equilibria calculated by Johnson et al. (2003) for an average metapelitic bulk rock composition akin to the sillimanite gneiss, the corresponding IP1 is located around 3.5 kbar and 650 °C in the P–T diagram of Fig. 6. However, lower pressure conditions for IP1 are expected due to the shift to lower temperature of the effective solidus of the rock caused by the involvement of boron from the breakdown of tourmaline during prograde metamorphism and migmatisation (cf. Pichavant, 1981). Therefore, a minimum pressure of 3 kbar for metamorphism and migmatisation is considered. The widespread retrograde muscovite in gneisses and migmatites, in which muscovite is thought to have partially formed by melt back-reactions, indicates crystallisation at pressures above that of IP1*. Moreover, these muscovites, coexisting with K-feldspar, biotite, and quartz, have Si contents close to 3.0 pfu (Table 2a). According to the corresponding geobarometer established by Massonne and Schreyer (1987), these Si contents point to pressures somewhat above 3 kbar under the provision that muscovite had formed at temperatures very close to that of the solidus curve. These geothermobarometric conclusions suggest a nearly isobaric path during medium to high-grade metamorphism and migmatisation.

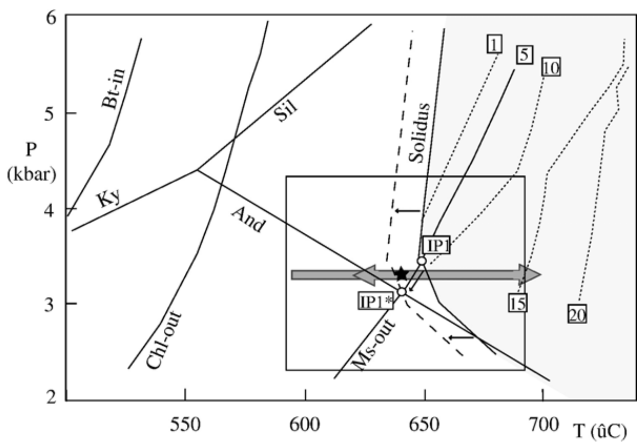

Fig. 6. Pressure–temperature pseudosection calculated for an average metapelitic composition (Johnson et al., 2003) in the $MnO–Na_2O–CaO–K_2O–FeO–MgO–Al_2O_3–SiO_2–H_2O$ system. Finely dashed lines and number in small squares indicate the percentage of melt produced during dehydration-melting reactions. The square indicates the P–T range calculated with garnet–biotite and GASP geothermobarometry. The dashed curve and arrows indicate the displacement of the solidus after the breakdown of tourmaline in metamorphic rocks. Thick arrows show the probable isobaric pressure–temperature path during high-grade metamorphism and migmatisation.

Table 4
Chemical analyses of rocks from the Puerto Edén Igneous and Metamorphic Complex (PEIMC)

Sample lithology	BG00-04	CPA00-23	YEK00-05	PE00-35	DE00-07	IC00-09	FF99-09A	DE00-48A	PE99-32D	PE99-32A	DE00-44	BG00-13RT	BG00-13L	BG00-13M
	Bt–Hbl–(Aln) granitoids	Granodiorite	Granodiorite	Tonalite	Porphyritic	Coarse-grained	Bt	Ms–Grt	Grt–Tur	Sillimanite	Andalusite	Migmatite	Leucosome	Melanosome
	Granodiorite				Monzogranite	Gneiss	Granite	Leucogranite	Leucogranite	Gneiss	Schist	Whole rock		
SiO_2	66.54	62.50	66.05	61.05	70.96	71.96	71.80	75.30	75.40	61.70	67.93	69.20	77.94	47.42
TiO_2	0.52	0.48	0.43	0.65	0.29	0.35	0.29	0.01	0.04	1.00	0.79	0.66	0.15	1.71
Al_2O_3	15.07	16.50	16.20	17.13	14.81	14.43	15.11	14.35	14.85	18.73	15.93	15.65	14.06	23.29
Fe_2O_3	0.95	1.74	1.62	1.02	0.11	0.61	0.18	0.48	0.30	1.04	0.67	0.86	0.28	1.18
FeO	3.52	3.16	2.52	5.04	2.80	2.20	2.23	0.20	0.38	5.48	4.72	3.78	0.63	9.79
MnO	0.08	0.12	0.13	0.15	0.06	0.04	0.04	0.05	0.03	0.06	0.06	0.05	0.01	0.14
MgO	1.72	2.39	1.38	3.07	0.74	0.72	0.65	0.10	0.33	2.29	1.69	1.63	0.41	3.90
CaO	4.21	4.96	4.32	5.83	2.56	1.33	1.68	0.30	0.49	0.64	0.81	0.19	0.28	0.21
Na_2O	2.57	2.80	3.19	1.91	3.59	2.83	2.65	3.82	4.13	1.83	1.98	1.30	2.28	1.30
K_2O	2.79	2.62	2.92	2.26	2.68	4.13	4.54	4.34	3.10	3.78	2.84	3.21	2.32	4.76
P_2O_5	0.08	0.20	0.14	0.21	0.12	0.10	0.04	0.07	0.31	0.10	0.13	0.10	0.07	0.05
LOI	1.70	2.49	1.05	1.61	0.91	0.89	0.57	0.72	0.77	2.91	2.37	2.94	1.39	5.92
Total	99.75	99.96	99.95	99.93	99.63	99.59	99.78	99.74	100.13	99.56	99.92	99.57	99.82	99.67
La	43	35	36	27	34	33	31	12	2	48	41	35	11	68
Ce	89	69	73	56	67	67	66	27	5	114	96	69	20	153
Nd	34	28	28	27	30	30	31	13	3	47	39	33	9	66

Sm	5	4	5	4	6	6	6	3	1	10	8	6	2	12
Eu	1	1	1	1	1	1	1	0	0	2	1	1	1	2
Gd	4	3	4	4	4	4	5	3	1	7	6	5	2	9
Dy	5	3	4	4	4	4	5	3	1	7	7	5	3	9
Ho	1	1	1	1	1	1	1	0	0	1	1	1	1	2
Er	3	2	2	3	1	2	3	1	1	4	3	3	2	5
Yb	3	2	2	3	1	2	3	1	1	4	3	3	2	5
Lu	0	0	0	0	0	0	0	0	0	1	1	0	0	1
Y	24	14	19	23	16	20	26	15	6	34	30	24	14	42
Sc	15	14	8	22	10	9	8	2	5	19	15	8	2	25
Hf	4	3	4	3	4	5	3	3	1	10	8	5	1	14
Nb	4	4	4	5	6	7	4	5	7	14	10	2	2	5
Th	15	8	9	7	9	11	10	6	<2	14	11	12	4	26
Zn	53	50	53	71	62	51	30	32	8	107	90	49	6	119
Co	9	10	7	14	6	5	3	3	<2	10	15	10	2	19
Ni	8	5	5	13	9	6	2	4	<2	21	24	19	4	46
Ba	470	570	700	460	780	720	960	345	20	530	450	1190	1300	1180
Cr	41	22	12	28	17	12	6	10	4	90	74	60	2	152
V	69	118	63	209	30	39	18	7	7	143	110	102	16	280
Cu	5	8	10	53	3	18	4	2	10	11	11	43	14	25
Sr	182	600	450	484	220	131	125	115	20	119	140	90	184	70
Zr	124	104	138	76	152	168	104	42	20	290	260	220	45	550
SI	1.01	1.00	1.00	1.06	1.10	1.25	1.23	1.24	1.35	2.27	2.04	2.63	2.08	3.04
An	20	23	21	28	12	6	8	1	0					
FeO∗	4.46	4.85	4.02	6.06	2.94	2.79	2.41	0.64	0.65	6.64	5.46	4.71	0.90	11.58

Major element oxides in wt.%; trace elements in ppm.

ASI = alumina saturation index; An = normative %An; FeO* = FeO + 0.8998Fe_2O_3.

8. Geochemistry

Field and petrographic observations suggest that the schists and gneisses represent the protoliths for the migmatites. The question to be addressed is whether they also represent the source for the leucogranitic rocks and the igneous protolith of the coarse-grained gneisses, interpreted as orthogneisses by Watters (1964). Moreover, our geochemical study was aimed at determining if there is a chemical relation between the coarse-grained gneiss

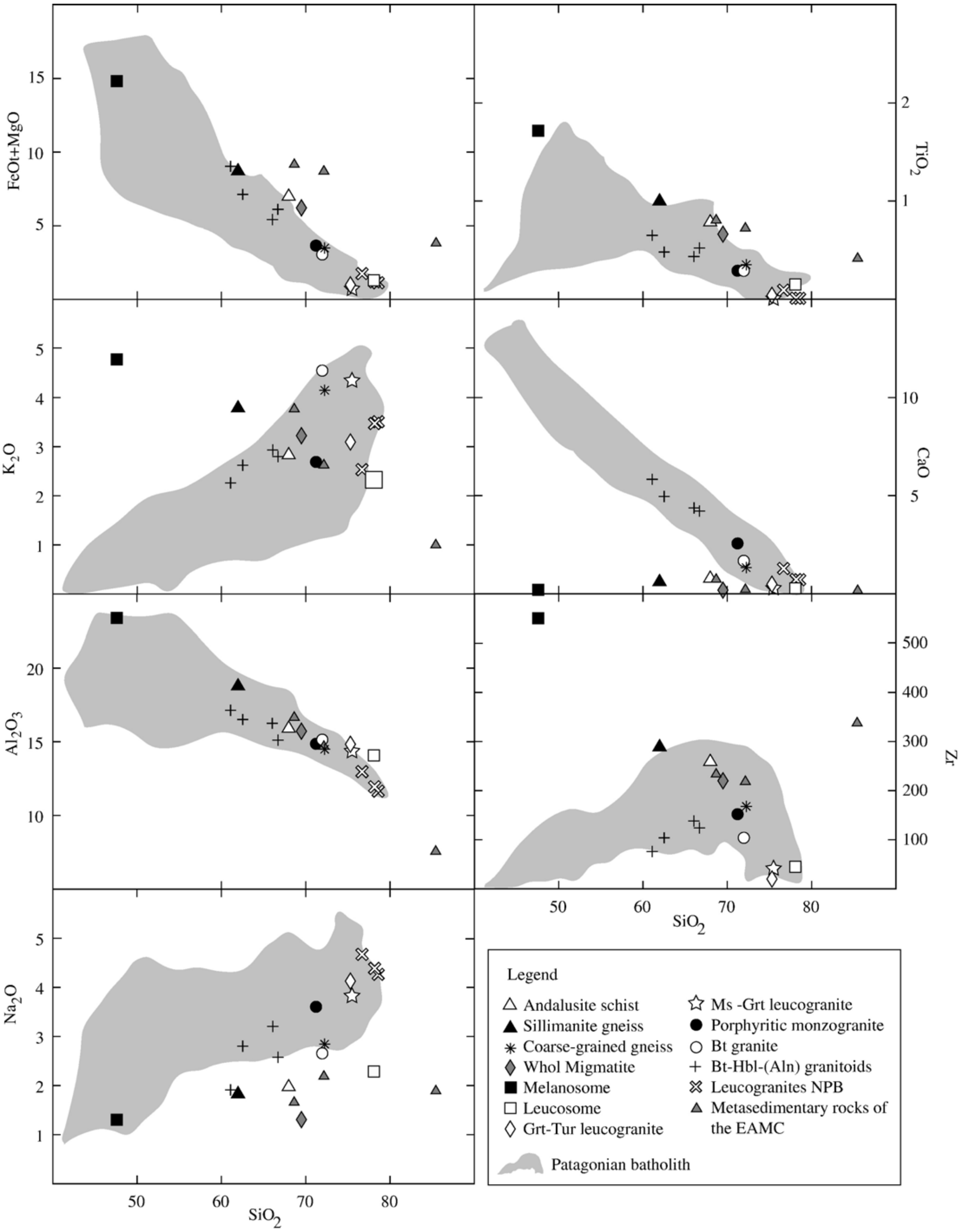

Fig. 7. Harker major element and Zr variation diagrams (Table 1). Patagonian batholith compositional field (shaded area) from Pankhurst et al. (1999) and Hervé (unpublished). Leucogranites at the North Patagonian batholith (NPB) from Hervé et al. (1993). Metasedimentary rocks from EAMC from Lacassie (2001).

and the porphyritic monzogranite, representing the main component of the Monte Albión composite pluton. Both the porphyritic monzogranite and the biotite granite are part of the biotite granitoid group.

8.1. Major and trace element compositions

Like subduction-related plutonic rocks from the continental margin, the biotite–hornblende–allanite granitoids and biotite granitoids are calc-alkaline in composition according to the FeO_T–MgO–(Na_2O+K_2O) plot (Kuno, 1968; not shown). The alumina saturation index (ASI value; Table 4) characterises the peraluminous character of the leucogranites (1.35–1.24), the coarse-grained gneiss and biotite granite (1.25–1.23), the porphyritic monzogranite (1.10) as well as the metaluminous character of biotite–hornblende–allanite granitoids (1.0–1.06).

Harker variation diagrams, including Zr (Fig. 7), show negative correlations with SiO_2 for (FeO∗+MgO), TiO_2, K_2O, and Al_2O_3 for the andalusite schist and sillimanite gneiss and for the low- to medium-grade metasedimentary rocks of the EAMC (48°S; analyses from Lacassie, 2001). The Zr content of these rocks shows a negative trend, except for the rock richest in SiO_2 (quartz-rich metagreywacke from EAMC). Noticeable is the high Zr content in the melanosome. Major oxides in metamorphic rocks can plot outside the compositional field for rocks of the Patagonian batholith.

The leucogranites and the leucosome have similarly low contents of major oxides and Zr, except for contents of K_2O and Na_2O which are higher in the muscovite–garnet and garnet–tourmaline leucogranites than in the leucosome. Compared to the other rocks, both leucogranites have very high Na_2O contents (much higher than in the metamorphic rocks).

The coarse-grained gneiss and the biotite granitoids (all with similar SiO_2 contents) plot within the compositional field of the Patagonian batholith (Pankhurst et al., 1999; Hervé, F., unpublished data). The biotite–hornblende–allanite granitoids show similar correlations of major oxides with SiO_2 to those shown by the batholithic rocks (Fig. 7).

8.2. REE compositions

The chondrite normalised (Sun and McDonough, 1989) rare earth element (REE) variation diagrams (Fig. 8) show consistent patterns among the metamorphic rocks with negative Eu anomalies. Fig. 8a shows the enriched nature of the melanosome relative to the sillimanite gneiss and andalusite schist. The counterpart is represented by the leucogranites (especially the garnet–

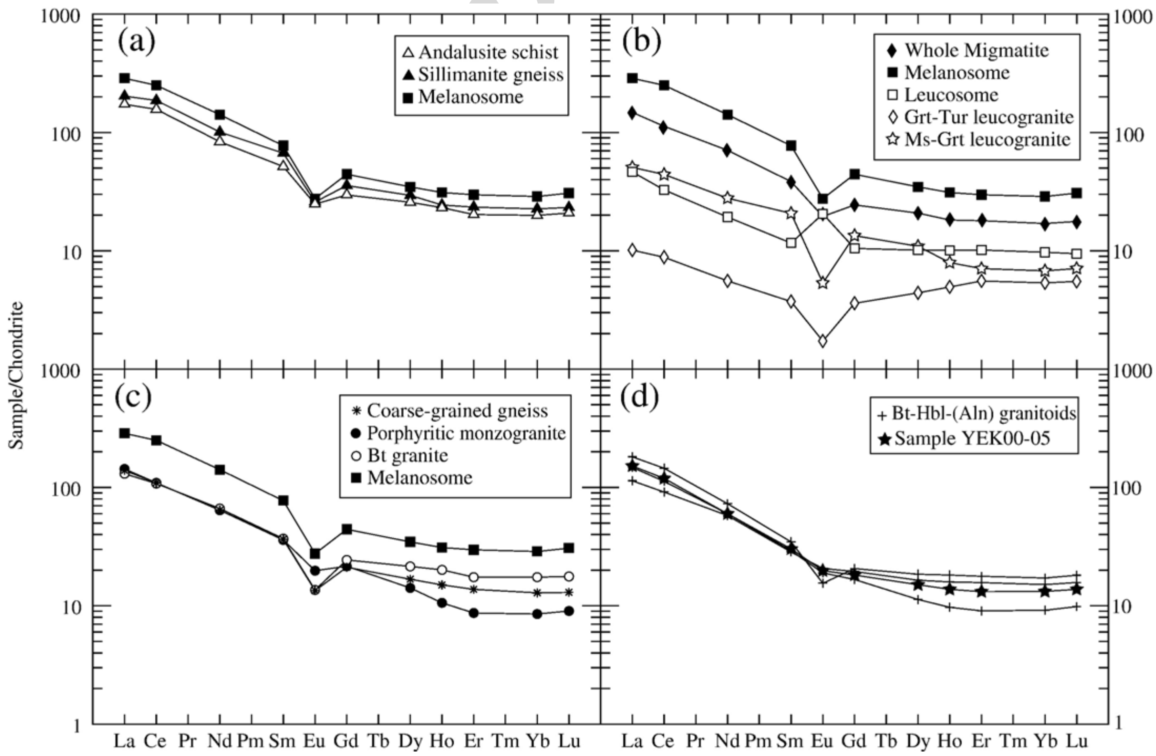

Fig. 8. Chondrite-normalized REE patterns of schists, gneisses, migmatites and granitoids.

tourmaline leucogranite) and the leucosome, which show relative depletion in REE (Fig. 8b). In the same figure (8a) the leucosome shows a positive Eu anomaly.

The coarse-grained gneiss, the biotite granitoids and the biotite–hornblende–allanite granitoids show similar REE patterns, the latter with a weak or no negative Eu anomaly. All these rocks are depleted with respect to the andalusite schist and the sillimanite gneiss (Fig. 8c,d).

9. Age and initial Sr and Nd isotope compositions

Metamorphic overgrowth zones in detrital zircons from the sillimanite gneiss (sample PE99-32A) record a Late-Jurassic age at ~ 150 Ma (Hervé et al., 2003) considered to be the age of high-grade metamorphism and migmatisation. This age coincides with the crystallisation age of 151 ± 1 Ma for the biotite granite (sample FF99-09; Martin et al., 2001) located ca. 30 km south-east from Puerto Edén. The sillimanite gneiss is in contact with the Monte Albión composite pluton (Fig. 1b) for which a similar crystallisation age is considered (see discussion).

As K–Ar ages of 102 ± 2 Ma for the porphyritic monzogranite, the muscovite–garnet leucogranite and the biotite–hornblende–allanite granodiorite and K–Ar biotite ages of 109 ± 3 Ma for the schists and gneisses (Calderón, 2005) are significantly younger than the U–Pb ages, they are considered as either cooling ages or reset ages during the Early Cretaceous emplacement of SPB magmas. Whole rock Rb–Sr and Sm–Nd isotope composition are shown in Table 5.

Both metasedimentary rocks yielded $^{87}Sr/^{86}Sr$ ratios (calculated for 150 Ma = Sr_0) of 0.7156 (andalusite schist) and 0.7134 (sillimanite gneiss), and correspondingly low initial εNd_{150} values of −7.6 and −7.1, respectively. The εNd_{150} are similar to those shown by low-grade metasedimentary rocks from the EAMC at ca. 48°S (εNd_{150} between −6.5 to −8.6; values calculated from Nd isotope data reported by Augustsson and Bahlburg, 2003). At 150 Ma, the coarse-grained gneiss and the biotite granite have slightly less radiogenic Sr and more radiogenic Nd, but they are indistinguishable from each other (Sr_0 of 0.7089, and εNd_{150} values of −4.4 and −4.9, respectively). At 100 Ma, the coarse-grained gneiss has a higher Sr_0 (0.7116) and lower εNd_{100} (−4.9). The porphyritic monzogranite, independent of the age, has the lowest Sr_0 in this group (0.7073–0.7081), but its εNd is very similar to the high-grade metasediments (εNd_{150} = −7.6 and εNd_{100} = −8.1).

Table 5
Rb–Sr and Sm–Nd isotopic compositions of the analysed rocks

Sample	Rb (ppm)	Sr (ppm)	Rb/Sr (wt)	$^{87}Rb/^{86}Sr$	$^{87}Sr/^{86}Sr$	$^{87}Sr/^{86}Sr$ (150 Ma)	$^{87}Sr/^{86}Sr$ (100 Ma)	εSr (150 Ma)	εSr (100 Ma)	T_{Bulk} (Ma)
DE00-44	137	149	0.9240	2.677	0.72130	0.71559	0.71750	160	186	455
PE99-32A	187	130	1.4377	4.166	0.72227	0.71338	0.71635	129	170	306
IC00-09	185	142	1.3000	3.765	0.71696	0.70894	0.71161	66	103	238
FF99-09A	171	137	1.2538	3.631	0.71659	0.70885	0.71143	64	100	240
PE99-32D	106	20	5.2475	15.238	0.74515	0.71266	0.72350	118	271	189
DE00-07	95	237	0.4009	1.160	0.70976	0.70728	0.70811	42	53	343
DE00-48A	165	119	1.3831	4.003	0.71235	0.70381	0.70666	−7	32	141
YEK00-05	119	486	0.2439	0.706	0.70593	0.70443	0.70493	1	8	162

Sample	Sm (ppm)	Nd (ppm)	$^{147}Sm/^{144}Nd$	$^{143}Nd/^{144}Nd$	$^{143}Nd/^{144}Nd$ (150 Ma)	$^{143}Nd/^{144}Nd$ (100 Ma)	εNd (150 Ma)	εNd (100 Ma)	T_{DM} (Ma)	T_{DM}* (Ma)
DE00-44	7.250	35.591	0.12314	0.512176	0.512055	0.512095	−7.6	−8.1	1408	1556
PE99-32A	8.465	41.815	0.12237	0.512202	0.512082	0.512122	−7.1	−7.6	1358	1519
IC00-09	5.399	26.280	0.12419	0.512342	0.512220	0.512261	−4.4	−4.9	1169	1321
FF99-09A	5.732	25.641	0.13514	0.512327	0.512194	0.512096	−4.9	−5.3	1339	1359
PE99-32D	0.613	1.556	0.23816	0.512348	0.512114	0.512239	−6.5	−6.2	−7782	1474
DE00-07	5.733	28.413	0.12197	0.512176	0.512056	0.512192	−7.6	−8.1	1392	1555
DE00-48A	5.013	20.378	0.14872	0.512512	0.512366	0.512415	−1.5	−1.8	1206	1098
YEK00-05	4.879	19.887	0.14831	0.512472	0.512326	0.512375	−2.3	−2.6	1280	1160

Samples and Geochronology (see text for references).
DE00-44 = andalusite schist (105 ± 3 Ma, K–Ar in Bt); PE99-32A = sillimanite gneiss (~ 150 Ma, U–Pb SHRIMP and 109 ± 3 Ma, K–Ar in Bt).
IC00-09 = coarse-grained gneiss (109 ± 3 Ma, K–Ar in Bt); FF99-09A = biotite granite (151 ± 1 Ma, U–Pb SHRIMP).
DE00-07 = porphyritic monzogranite (102 ± 2, K–Ar in Bt); DE00-48A = Ms–Grt leucogranite (102 ± 2, K–Ar in WM).
YEK00-05 = Bt–Hbl–(Aln) granodiorite (102 ± 2 Ma, K–Ar in Bt).
Nd Model ages : T_{DM} conventional depleted mantle model age; T_{DM}* crust-derived model age (DePaolo et al., 1991).

There are similarities between the isotopic compositions of the muscovite–garnet leucogranite and the biotite–hornblende–allanite granodiorite. For the leucogranite at 100 Ma, Sr_0 is 0.7067 and εNdt −1.8. In the case of the biotite–hornblende–allanite granodiorite Sr_0 is 0.7049 and εNdt −2.6. For 150 Ma lower values result.

The metasedimentary rocks show depleted mantle model ages (T_{DM}) of 1408 (andalusite schist) to 1358 (sillimanite gneiss) Ma. Similar ages of 1339 Ma and 1392 Ma were obtained for the biotite granite and the porphyritic monzogranite, respectively, but the T_{DM} model age of the coarse-grained gneiss is younger (1169 Ma). The muscovite–garnet leucogranite also has a younger T_{DM} of 1206 Ma compared to the biotite–hornblende–allanite granodiorite (1280 Ma). Models that incorporate an additional stage of crustal residence after differentiation from the depleted mantle but preceding the formation of the final rock ('crust-derived' model ages, DePaolo et al., 1991) are included in Table 5 (T_{DM}*). They show that the high-grade metamorphic rocks and the porphyritic monzogranite can have similar T_{DM}* model ages of 1520–1560 Ma. The coarse-grained gneiss and biotite granite gives younger values of 1320–1360. The muscovite–garnet leucogranite and biotite–hornblende–allanite granodiorite yielded the youngest T_{DM}* model ages of ca. 1100–1160 Ma.

10. Discussion

The studied suite of rocks represents different elements of an anatectic system. Their mineral and whole rock chemical and isotopic compositions allow us to explore processes linked to the low-pressure amphibolite facies metamorphism and partial melting of aluminous metapelitic rocks. They also allow us to follow major and trace element behaviour during migmatisation and to test the possible link between high-grade metamorphism and the genesis of large granitic bodies. An important assumption about the evolution of anatexis in the PEIMC is that isotopic equilibrium existed during the processes involved (partial melting, assimilation and fractional crystallisation during non-coaxial flow).

10.1. Mineral and chemical redistribution during migmatisation

The observed partial melting processes are probably dominated by muscovite and biotite dehydration-melting reactions. Major elements are thought to be redistributed among major reactant phases, peritectic minerals and the melt phase during this process. During anatexis many trace elements (e.g. Zr and REE) are partitioned in accessory phases and melt. According to Bea (1996) such trace elements show a non-Henryan behaviour because these accessory phases are preferentially included in major minerals and, thus, cannot equilibrate with the melt. However, other reasons for the non-Henryan behaviour are also conceivable. Considering the composition of REE-bearing accessory minerals in metasedimentary rocks undergoing anatexis, it is expected that the LREE budget is dominated by monazite and allanite. The HREE behaviour, however, is controlled by apatite, monazite, zircon and garnet, whereas the MREE budget is due to the distribution of these elements between monazite, apatite and garnet (Bea, 1996; Ayres and Harris, 1997; Pressley and Brown, 1999).

The sillimanite gneiss (without leucosomes) shows a slight enrichment in K_2O, FeO*, MgO, TiO_2, Al_2O_3 and REE and a depletion in CaO, Na_2O, Sr and Eu relative to the andalusite schist (Fig. 8a). Thus, the sillimanite gneiss is richer in biotite and poorer in plagioclase compared to the andalusite schist. This could be the result of the peritectic reaction muscovite + plagioclase + quartz = melt + K-feldspar + sillimanite + biotite which has taken place in the sillimanite gneiss to enrich it with biotite (restite).

According to field relations it seemed to be likely that the granitic melt (leucosomes), formed in sillimanite gneiss, migrated into fault zones to crystallize as garnet–tourmaline leucogranitic dykes. However, we observed that there is a pronounced negative Eu anomaly in the leucogranite and a positive Eu anomaly in the leucosome of the migmatite (Fig. 8b). This would at the first glance contradict our above idea based on field relations. Nevertheless, we can conceive a process for the contrasting Eu anomalies. It might be possible that the original granitic melt in the sillimanite gneiss started to crystallize first to plagioclase where Eu is enriched. Then the remaining melt migrated into the fault zones. The leucosome enriched in plagioclase would then show a positive Eu anomaly but the granites crystallised as dykes would exhibit a negative Eu anomaly as observed. The strong REE depletion of the garnet–tourmaline leucogranite relative to the sillimanite gneiss could be the result of the retention of REE-bearing accessory phases in biotite selvedges of the sillimanite gneiss. In this scenario, sillimanite gneisses with concordant and discordant garnet–tourmaline leucogranite veins and dykes represent the partially modified migmatitic source or mesosome of the leucogranite and could be, thus, considered as metatexites.

In the same way we can explain the Sr-enrichment of the leucosome in the migmatite which is rich in plagioclase (Fig. 8b). The low K_2O content in the leucosome must be due to: (1) the migration of more evolved melts from their place of generation (e.g. Milord et al., 2001). (2) K_2O loss within the fluid phase released from leucosome during its cooling below the solidus (e.g. Kriegsman, 2001). This process could adduce to the slight enrichment in K_2O and muscovite crystallisation in the melanosome. (3) Enrichment of K in the restite due to the peritectic reaction given above. Indeed, the melanosome is strongly enriched in biotite components (K_2O, FeO*, MgO and TiO_2), Zr and REE (Figs. 7 and 8b). The latter elements reflect the inclusion of accessory phases (zircon) in biotite and their accumulation during prograde migmatisation. The LREE pattern of the melanosome proves the presence of a mineral that enriches LREE. This could be either monazite, although not observed in the migmatite, or allanite or an unexpected LREE-bearing composition of apatite hosted in the melanosome. Due to the higher proportion of the melanosome relative to the leucosome in the migmatite (Fig. 2e) this rock is considered as a stromatite with high proportion of melanosome formed after pervasive partial melt back-reactions and retrograde (chlorite formation) metamorphism.

The presence of quartz inclusions and schlieren of biotite and sillimanite in the coarse-grained gneiss could reflect the residual character after partial melting of metasedimentary rocks in the biotite stability field. This implies that coarse-grained quartz-bands in the metasedimentary source (similar to those in the andalusite schists; Fig. 2a) were hardly molten during the anatectic process and the schlieren represent a restite rich in peritectic biotite and sillimanite (e.g. Sawyer, 1998; Milord et al., 2001). The leucosome (former granitic melts) underwent deformation at subsolidus conditions after cooling. The evidence for this is (1) strain shadows around quartz-rich inclusions, (2) a weak foliation which, however, can also be strong and concentrated in mylonitic zones. The coarse-grained gneiss considered by Watters (1964) as an orthogneiss is, thus, considered here as a foliated leucodiatexite.

Coarse-grained gneiss and biotite granitoids show similar LREE contents, but the porphyritic monzogranite shows the least negative Eu-anomaly compatible with a high content of plagioclase in the rock. The difference in HREE contents among these rocks (Fig. 8c) could be related (1) to the retention of zircon, apatite and garnet in the restite of the source of the granitic melts, (2) to their incorporation as solid fraction in the granitic melt or their crystallisation from the granitic melt after partial dissolution from the source. The REE patterns are slightly depleted with respect to the metamorphic rocks, which is consistent with the diatexite model characterised by the generation of residuum-bearing granitic rocks (cf. Sawyer, 1998). The high Ca content of these rocks relative to the metamorphic rocks and the leucogranites could be explained either by anatectic processes dominated by plagioclase-consuming H_2O-fluxed reactions, such as muscovite + plagioclase + quartz + H_2O = melt (cf. Otamendi and Patiño Douce, 2001), or by protolith variations in the source rocks of the melts.

10.2. Isotopic signature and petrogenetic implications

The Nd isotope composition of the high-grade metasedimentary rocks is consistent with the range of εNd_{150} values between −6.5 and −8.6 for low-grade metasedimentary rocks of the EAMC (judging from the Nd data reported by Augustsson and Bahlburg, 2003). The initial Sr and Nd compositions of the high-grade metapelitic rocks are consistent with those of the EAMC rocks studied by Weaver et al. (1990), albeit these rocks show somewhat lower εNd_{150} values (−4.3 to −6.3; Fig. 9). Therefore, it seems to be likely that the source region of the migmatites at 150 Ma was isotopically more variable than presented by the two high-grade metasedimentary rocks.

The mineralogical, chemical and Sr–Nd isotopic similarities, shown by the coarse-grained gneiss and the biotite granite (see Tables 2a and 2b), imply a common protolith for these two rocks prior to 150 Ma, the age of high-grade metamorphism and crystallisation of the granite. Their Sr_0 (~ 0.709) and εNd_{150} values (−4.4, −4.9) are lower and higher, respectively, than those of

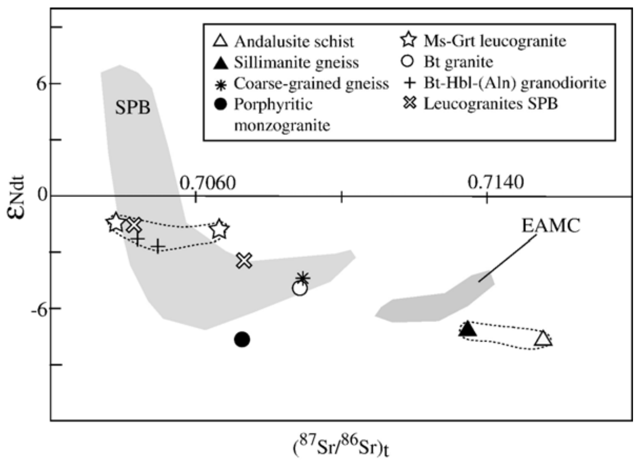

Fig. 9. Initial $^{87}Sr/^{86}Sr$ vs. εNd values of the studied samples. Isotope composition of the Ms–Grt leucogranite and the Bt–Hbl–Aln granodiorite calculated either at 100 Ma or at 150 Ma are shown. Two mid-Cretaceous two-mica leucogranites from the SPB and the SPB and EAMC compositional fields at 48°S were taken from Weaver et al. (1990).

the sillimanite gneiss, but are still indicative of a significant metasedimentary component. Thus, it is reasonable that the constituents of the coarse-grained gneiss were generated mainly by anatexis of metapelitic rocks during the Late Jurassic high-temperature, low-pressure metamorphism and that a similar petrogenesis applies to the biotite granite.

The porphyritic monzogranite has even a lower Sr_0 (0.7073) than the coarse-grained gneiss and the biotite granite, but its εNd_{150} value of −7.6 is indistinguishable from those of the high-grade metamorphic rocks. The lower Sr_0 value could, for instance, imply that the source of the porphyritic monzogranite contained more basic material than that of the biotite granite.

Although the real crystallisation age of the porphyritic monzogranite (main constituent of the Monte Albión composite pluton) and its cooling history are not well known, the strikingly similar Sm and Nd contents compared to the coarse-grained gneiss and biotite granite, the preservation of small schlieren of anhedral biotite and because it is delimited to the north and south by migmatitic rocks, we postulate a common process for their genesis and hence assume a Late Jurassic age of crystallisation.

Until this point, the strongly peraluminous muscovite–garnet leucogranite has been considered as being produced by muscovite dehydration-melting reactions in metapelites. However, the Sr–Nd isotopic signature especially at 150 Ma is by far too primitive to allow formation exclusively by anatexis of the Palaeozoic metasedimentary rocks (e.g. andalusite schist, Table 5). It is comparable in these respects with mid-Cretaceous two-mica leucogranites of the SPB (Fig. 9), which have been interpreted as generated through partial melting of earlier contaminated plutons, and not by partial melting of the metasedimentary basement rocks (Weaver et al., 1990). Because the muscovite–garnet leucogranite has a Sr–Nd isotopic signature similar to the biotite–hornblende–allanite granodiorite, both plutonic rocks could be petrogenetically related. Both rocks gave K–Ar mineral ages of ca. 102 Ma (Calderón, 2005).

10.3. Geodynamic constraints

Because leucosomes are located in structurally controlled sites within the migmatites, such as interboudin partitions, strain shadows, fractures and fold hinge zones, melt flow through the migmatites during deformation is widely suggested (e.g. Brown and Rushmer, 1997; Marchildon and Brown, 2001; Vanderhaeghe, 2001; Solar and Brown, 2001). The parallelism of leucosome and the foliation in mesosome, the leucosome distribution in stromatites defining S–C-type structures (Fig. 2e) and the network of leucogranite dykes concordant and oblique to the foliation in sillimanite gneisses (Fig. 2f) are indicative of syn-deformational migmatisation. During the deformation event subvertical east-dipping S_2 composite foliation, subparallel to the axial plane of tight folds of quartz bands, developed pointing to a kilometre-sized upright fold with present-day subvertical- to west-vergent axial surface. Microstructures in schists and gneisses indicate deformation processes acting late during or even after the peak metamorphic P–T conditions were attained. Nevertheless, it is likely that composite foliation and mylonite development at temperatures between 400 and 500 °C occurred during the latest stages of the Late Jurassic crustal anatectic event. The Albian minimum age (see Section 9) is related to the development of shear zones as temperatures of dynamic recrystallisation seen in microstructures and the closure temperature (ca. 300–400 °C) of the K–Ar system for biotite and muscovite are similar.

Areas with sillimanite gneisses, migmatites and leucogranites (Fig. 1) are interpreted as melt drainage systems for melt migration during shearing-enhanced melt-extraction processes at crustal depths of ca. 10 km. For the Monte Albión composite pluton, which has an N–S trending ellipsoidal shape and shows locally, aligned K-feldspar megacrysts defining a subvertical magmatic foliation, a syntectonic origin is suggested considering a parautochthonous kilometre-sized batch of melt emplaced within sillimanite gneisses in a higher structural level in the crust.

Massonne et al. (2004) have been determined crystallisation depths of ca. 20 km for Late Jurassic garnet–muscovite granites located in the eastern margin of the batholith. Hence, the migration of granitic melts may have occurred between depths of 20 and 10 km in the continental crust along shear zones with associated folds and fractures. The continental crust in total was probably thickened in areas of granitic plutonism. The corresponding process was coeval with the emplacement of mafic magmas in the Rocas Verdes basin in a zone in which upper-crust extensional tectonics is well documented. Consequently, the magmatic accretion of mantle derived magmas and their injection within the upper continental crust is a possible heat source for crustal anatexis.

11. Conclusions

On the basis of the previous discussion, we think that the subsequent scenario for the evolution of schists, gneisses, migmatites and biotite-bearing granitoids of the PEIMC is justified: (1) the temperature increase from andalusite schists through sillimanite gneisses to migmatites caused low degrees of partial melting driven mainly by decomposition of muscovite. Peritectic biotite and sillimanite formed during the corresponding reactions and were concentrated in the melanosomes. REE were enriched in the melanosomes due to zircon accumulation in biotite selvedges. (2) REE-depleted leucogranites, produced during the early stage of migmatisation, were first segregated within the gneissic domains and afterwards, due to deformation, segregated through syn-deformational dilatational domains. Crystal fractionation processes are evidenced by compositional differences between leucosome (with Eu positive anomaly) and garnet–tourmaline leucogranite (with Eu negative anomaly). The original granitic melt started to crystallize first to quartz and plagioclase, mostly oligoclase in composition, where Eu is enriched. Subsequently, the remaining melt migrated into dilatational sites and crystallizes as leucogranite dykes in which plagioclase is albite in composition. (3) An anatectic origin of the porphyritic monzogranite is suggested by the Nd signature (εNd_{150} value of -8.1) which is indistinguishable from those of the high-grade metamorphic rocks (εNd_{150} value of -7.6 and -8.1). Nevertheless, the isotopic composition of the coarse-grained gneiss ($\varepsilon Nd_{150} = -4.4$) and the biotite granite ($\varepsilon Nd_{150} = -4.9$) indicates the mixing of components derived from a heterogeneous source. (4) The biotite–hornblende–allanite granitoids and the muscovite–garnet leucogranite, also formed by partial melting of crustal components, are probably Early Cretaceous in age and do not have a direct genetic relation to the Late Jurassic crustal anatectic event.

The PEIMC represents a crustal-scale shear zone in which high-temperature–low-pressure metamorphism and migmatisation of metapelites, ductile shearing and melt extraction processes have been involved in the formation of Late Jurassic composite plutons of the South Patagonian batholith. Late Jurassic biotite gneisses and granitoids represent fertile lithologies for crustal contamination within the Cretaceous to Cenozoic subduction-related magmatic arc.

Acknowledgements

This work was supported by Fondecyt 1010412 grant to F. Hervé, Conicyt–BMBF (CHL 99/031) grant to F. Hervé and H.-J. Massonne, MCT-PRONEX (167/96) grant to C. Tassinari, the Conicyt BAPRTD and Beca PG/61/2001 to M. Calderón and a Leverhulme Trust Emeritus Fellowship to R.J. Pankhurst. We thank J. Otamendi, G. Solar and an anonymous reviewer for their critical and constructive reviews of this manuscript. We thank M. Holdaway for sending us the GBGASP geothermobarometer program and comments. Sample W107 was gently provided by Bill Watters. M. Calderón would like to thank S. Nettle, C. Tascón, M. Mansilla, Puerto Edén community and to the "Timao" of the Centro de Pesquisas Geocronológicas (USP) for their aid and hospitality during different stages of this research.

References

Augustsson, C., Bahlburg, H., 2003. Active or passive continental margin? Geochemical and Nd isotope constraints of metasediments in the backstop of a pre-Andean accretionary wedge in southernmost Chile (4630–4830S). In: McCann, T., Saintot, A. (Eds.), Tracing tectonic deformation using the sedimentary record. Special Publication, vol. 280. Geological Society, Boulder, Colorado, pp. 253–268.

Ayres, M., Harris, N., 1997. REE fractionation and Nd-isotope disequilibrium during crustal anatexis: constraints from Himalayan leucogranites. Chemical Geology 139, 249–269.

Bea, F., 1996. Residence of REE, Y, Th and U in granites and crustal protoliths; implications for the chemistry of crustal melts. Journal of Petrology 37, 521–552.

Brown, M., 1973. The definition of metatexis, diatexis and migmatite. Proceedings of the Geologist's Association 84, 371–382.

Brown, M., D'Lemos, R.S., 1991. The Cadomian granites of Mancellia, north-east Amorican massif of France: relationship to the St. Malo migmatite belt, petrogenesis and tectonic setting. Precambrian Research 51, 393–427.

Brown, M., Rushmer, T., 1997. The role of deformation in the movement of granitic melt: views from the laboratory and the field. In: Holness, M.B. (Ed.), Deformation-enhanced Fluid Transport in the Earth's Crust and Mantle. Chapman and Hall, London, pp. 111–144.

Brown, M., Solar, G.S., 1998. Shear zone systems and melts: feedback relations and self-organization in orogenic belts. Journal of Structural Geology 20, 211–227.

Bruce, B., Nelson, E.P., Weaver, S.G., Lux, D.R., 1991. Temporal and spatial variations in the southern Patagonian batholith: constraints on magmatic arc development. In: Harmon, R.S., Rapela, C.W. (Eds.), Andean magmatism and its tectonic setting. Special Paper, vol. 265. Geological Society of America, Boulder, Colorado, pp. 1–12.

Calderón, M., 2005. Metamorfismo de alta temperatura y baja presión en rocas del basamento metamórfico en Puerto Edén. MsC Thesis, Departamento de Geología, Universidad de Chile.

Calderón, M., 2006. Petrogenesis and tectonic evolution of Late Jurassic bimodal magmatic suites (Sarmiento Complex) and migmatites (Puerto Edén Igneous Metamorphic Complex) in the southern Patagonian Andes, Chile. PhD Thesis, 170 pp.

Calderón, M., Hervé, F., 2000. Metamorfismo de contacto en el margen oriental del batolito Sur-Patagónico. IX Congreso Geológico Chileno 2, 707–711.

Dalziel, I.W.D., 1981. Back-arc extension in the southern Andes: a review and critical reappraisal. Royal Society of London Philosophical Transactions, Series A 300, 319–335.

DePaolo, D.J., Linn, A.M., Schubert, G., 1991. The continental crustal age distribution; methods of determining mantle separation ages from Sm–Nd isotopic data and application to the Southwestern United States. Journal of Geophysical Research B96, 2071–2088.

Faúndez, V., Hervé, F., Lacassie, J.P., 2002. Provenance and depositional setting of pre-Late Jurassic turbidite complexes in

Patagonia, Chile. New Zealand Journal of Geology and Geophysics 45, 411–425.
Greenfield, J.E., Clarke, G.L., Bland, M., Clarke, D.J., 1996. In-situ migmatite and hybrid diatexite at Mt. Stafford, central Australia. Journal of Metamorphic Geology 14, 413–426.
Hanson, R.E., Wilson, T., 1993. Large-scale rhyolite peperites (Jurassic, southern Chile). Journal of Volcanology and Geothermal Research 54, 247–264.
Hervé, F., 1993. Paleozoic metamorphic complexes in the Andes of Aysén, southern Chile (west of? Occidentalia). In: Ortega Gutiérrez, F., Coney, P.j., Centeno García, E., Gomez-Caballero (Eds.), Proceedings of the First Circum-Pacific and Circum-Atlantic Terrane Conference, Guanajuato, Mexico, pp. 64–65.
Hervé, F., Aguirre, L., Godoy, E., Massonne, H., Morata, D., Pankhurst, R.J., Ramírez, E., Sepúlveda, V., Willner, A., 1998. Nuevos antecedentes acerca de la edad y las condiciones P–T de los complejos metamórficos en Aysén, Chile. X Congreso Latinoamericano de Geología y VI Congreso Nacional de Geología Económica, Buenos Aires, Argentina, vol. 2, pp. 134–137.
Hervé, F., Fanning, C.M., Pankhurst, R.J., 2003. Detrital zircon age patterns and provenance of the metamorphic complexes of southern Chile. Journal of South American Earth Sciences 16, 107–123.
Holdaway, M.J., 2000. Application of new experimental and garnet Margules data to the garnet–biotite geothermometer. American Mineralogist 85, 881–892.
Holdaway, M.J., 2001. Recalibration of the GASP geobarometer in light of recent garnet and plagioclase activity models and versions of the garnet–biotite geothermometer. American Mineralogist 86, 1117–1129.
Johnson, T.E., Brown, M., Solar, G.S., 2003. Low-pressure subsolidus and suprasolidus phase equilibria in the MnNCKFMASH system: constraints on conditions of regional metamorphism in western Maine, northern Appalachians. American Mineralogist 88, 624–638.
Kriegsman, L.M., 2001. Partial melting, partial melt extraction and partial back reaction in anatectic migmatites. Lithos 56, 75–96.
Kuno, H., 1968. Origin of andesite and its bearing on the island arc structure. Bulletin Volcanologique 32, 141–176.
Labotka, T.C., 1991. Chemical and physical properties of fluids. In: Kerrick, D.M. (Ed.), Contact Metamorphism, Mineralogical Society of America, Reviews in Mineralogy, vol. 3, pp. 43–97.
Lacassie, J.P., 2001. Geología del interfluvio Baker-Bravo (47°30′–48°S), Aysén, Chile. Graduation Thesis, Departamento de Geología, Universidad de Chile.
Marchildon, N., Brown, M., 2001. Melt segregation in late syntectonic anatectic migmatites: an example from the Onawa contact aureole, Maine, USA. Physics and Chemistry of the Earth (A) 26 (4–5), 225–229.
Martin, M., Pankhurst, R.J., Fanning, C.M., Thomson, S.N., Calderón, M., Hervé, F., 2001. Age distribution of plutons across the southern Patagonian batholith: new U–Pb data on zircons. III South American Symposium on Isotope Geology, Pucón, Chile, pp. 585–588. extended abstracts (CD).
Massonne, H.-J., Schreyer, W., 1987. Phengite geobarometry based on the limiting assemblage with K-feldspar, phlogopite, and quartz. Contributions to Mineralogy and Petrology 96, 212–224.
Massonne, H.-J., Calderón, M., Hervé, F., 2004. Magmatic muscovite and garnet in granites of the southern Patagonian batholith. In: Carcione, J., Donda, F., Lodolo, E. (Eds.), International Symposium on the Geology and Geophysics of the Southernmost Andes, the Scotia Arc and the Antarctic Peninsula, Buenos Aires, vol. 45. Bollettino di Geofisica teorica ed applicata, Argentina, pp. 121–125.
Milord, I., Sawyer, E.W., Brown, M., 2001. Formation of diatexite migmatite and granite magma during anatexis of semi-pelitic metasedimentary rocks: an example from St. Malo, France. Journal of Petrology 42, 487–505.
Mukasa, S.B., Dalziel, I.W.D., 1996. Southernmost Andes and South Georgia island, North Scotia ridge: zircon U–Pb and muscovite Ar/Ar age constraints on tectonic evolution of southwestern Gondwanaland. Journal of South American Earth Sciences 9, 349–365.
Nelson, E.P., Bruce, R., Elthon, D., Kammer, D., Weaver, S., 1988. Regional lithological variations in the Patagonian batholith. Journal of South American Earth Sciences 1 (3), 239–247.
Otamendi, J.E., Patiño Douce, A.E., 2001. Partial melting of aluminous metagreywackes in the northern Sierra Comechingones, Central Argentina. Journal of Petrology 42, 1751–1772.
Pankhurst, R.J., Leat, P.T., Sruoga, P., Rapela, C.W., Márquez, M., Storey, B.C., Riley, T.R., 1998. The Chon Aike province of Patagonia and related rocks in West Antarctica: a silicic large igneous province. Journal of Volcanology and Geothermal Research 81, 113–136.
Pankhurst, R.J., Weaver, S.D., Hervé, F., Larrondo, P., 1999. Mesozoic–Cenozoic evolution of the north Patagonian batholith in Aysén, southern Chile. Journal of Geological Society, London 156, 673–694.
Pankhurst, R.J., Riley, T.R., Fanning, M.C., Kelley, S.P., 2000. Episodic silicic volcanism in Patagonia and the Antarctic peninsula: chronology of magmatism associated with the break-up of Gondwana. Journal of Petrology 41 (5), 605–625.
Passchier, C.W., Trouw, R.A.J., 1996. Microtectonics. Springer-Verlag, Berlin Heidelberg.
Pattison, D.R.M., 1992. Stability of andalusite and sillimanite and the Al_2SiO_5 triple point: constraints from the Ballachulish aureole, Scotland. Journal of Geology 100, 423–446.
Pichavant, M., 1981. An experimental study of the effect of boron on a water saturated haplogranite at 1 kbar vapour pressure. Contribution to Mineralogy and Petrology 76, 430–439.
Pressley, R.A., Brown, M., 1999. The Phillips pluton, Maine, USA: evidence of heterogeneous crustal sources and implications for granite ascent and emplacement mechanisms in convergent orogens. Lithos 46, 335–366.
Ramírez, E., 2003. Geotermobarometría en metapelitas de los complejos metamórficos de Aysen, chile y sus implicancias tectónicas. PhD Thesis, Departamento de Geología, Universidad de Chile.
Sawyer, E.W., 1998. Formation and evolution of granite magmas during crustal reworking: the significance of diatexites. Journal of Petrology 39, 1147–1167.
Simpson, C., Wintsch, R.P., 1989. Evidence for deformation-induced K-feldspar replacement by myrmekite. Journal of Metamorphic Geology 7, 261–275.
Solar, G., Brown, M., 2001. Petrogenesis of migmatites in Maine, USA: possible source of peraluminous leucogranite in plutons? Journal of Petrology 42 (4), 789–823.
Spear, F.S., Kohn, M.J., Cheney, J.T., 1999. P–T paths from anatectic pelites. Contribution to Mineralogy and Petrology .134, 17–32.
Stern, C.R., Mukasa, S.B., Fuenzalida, R., 1992. Age and petrogenesis of the Sarmiento ophiolite complex of southern Chile. Journal of South American Earth Sciences 6, 97–104.
Sun, S., McDonough, W.F., 1989. Chemical and isotopic systematics of oceanic basalts: implications for mantle composition and processes. In: Saunders, A.D., Norris, M.J. (Eds.), Magmatism in the Ocean Basins. Geological Society, vol. 42. Special Publications, London, pp. 313–345.

Thomson, S.N., Hervé, F., Fanning, C.M., 2000. Combining fission-track and U–Pb SHRIMP zircon ages to establish stratigraphic and metamorphic ages in basement sedimentary rocks in southern Chile. IX Congreso Geológico Chileno, Puerto Varas, Chile, vol. 2, pp. 769–773.
Thomson, S.N., Hervé, F., 2002. New time constraints for the age of metamorphism at the ancestral Pacific Gondwana margin of southern Chile (42–52°S). Revista Geológica de Chile 29 (2), 255–271.
Vanderhaeghe, O., 2001. Melt segregation, pervasive melt migration and magma mobility in the continental crust: the structural record from pores to orogens. Physics and Chemistry of the Earth (A) 26 (4–5), 213–223.
Watters, W.A., 1964. Geological work at Puerto Edén, Wellington island, southern Chile. Transactions of the Royal Society of New Zealand. Geology 2 (11), 155–168.
Weaver, S.G., Bruce, B., Nelson, E.P., Brueckner, H.K., LeHuray, A.P., 1990. The Patagonian batholith at 48°S latitude, Chile: geochemical and isotopic variations. In: Harmon, R.S., Rapela, C.W. (Eds.), Andean Magmatism and its Tectonic Setting. Special Paper, vol. 241. Boulder, Colorado, Geological Society of America, pp. 33–50.
Weinberg, R., 1999. Mesoscale pervasive felsic magma migration: alternative to dyking. Lithos 46, 393–410.
Wimmenauer, W., Bryhni, I., 2002. Migmatites and related rocks. A proposal on behalf of the IUGS Subcommission on the Systematics of Metamorphic Rocks (Towards a unified nomenclature of metamorphic petrology). http://www.bgs.ac.uk/scmr/docs/paper_6 /scmr_mig.pdf.